



High-resolution mineral dust and sea ice proxy records from the Talos Dome ice core

S. Schüpbach^{1,2,3}, U. Federer^{1,2}, P. R. Kaufmann^{1,2}, S. Albani⁴, C. Barbante^{3,5}, T. F. Stocker^{1,2}, and H. Fischer^{1,2}

¹Climate and Environmental Physics, Physics Institute, University of Bern, Bern, Switzerland

²Oeschger Centre for Climate Change Research, University of Bern, Bern, Switzerland

³Environmental Sciences, Informatics and Statistics Department, University of Venice, Venice, Italy

⁴Department of Earth and Atmospheric Sciences, Cornell University, Ithaca, NY, USA

⁵Institute for the Dynamics of Environmental Processes – National Research Council, Venice, Italy

Correspondence to: S. Schüpbach (schuepbach@climate.unibe.ch)

Received: 31 May 2013 – Published in Clim. Past Discuss.: 21 June 2013

Revised: 8 November 2013 – Accepted: 27 November 2013 – Published: 23 December 2013

Abstract. In this study we report on new non-sea salt calcium (nssCa^{2+} , mineral dust proxy) and sea salt sodium (ssNa^+ , sea ice proxy) records along the East Antarctic Talos Dome deep ice core in centennial resolution reaching back 150 thousand years (ka) before present. During glacial conditions nssCa^{2+} fluxes in Talos Dome are strongly related to temperature as has been observed before in other deep Antarctic ice core records, and has been associated with synchronous changes in the main source region (southern South America) during climate variations in the last glacial. However, during warmer climate conditions Talos Dome mineral dust input is clearly elevated compared to other records mainly due to the contribution of additional local dust sources in the Ross Sea area. Based on a simple transport model, we compare nssCa^{2+} fluxes of different East Antarctic ice cores. From this multi-site comparison we conclude that changes in transport efficiency or atmospheric lifetime of dust particles do have a minor effect compared to source strength changes on the large-scale concentration changes observed in Antarctic ice cores during climate variations of the past 150 ka. Our transport model applied on ice core data is further validated by climate model data.

The availability of multiple East Antarctic nssCa^{2+} records also allows for a revision of a former estimate on the atmospheric CO_2 sensitivity to reduced dust induced iron fertilisation in the Southern Ocean during the transition from the Last Glacial Maximum to the Holocene (T1). While a former estimate based on the EPICA Dome C (EDC) record only suggested 20 ppm, we find that reduced dust induced iron fer-

tilisation in the Southern Ocean may be responsible for up to 40 ppm of the total atmospheric CO_2 increase during T1.

During the last interglacial, ssNa^+ levels of EDC and EPICA Dronning Maud Land (EDML) are only half of the Holocene levels, in line with higher temperatures during that period, indicating much reduced sea ice extent in the Atlantic as well as the Indian Ocean sector of the Southern Ocean. In contrast, Holocene ssNa^+ flux in Talos Dome is about the same as during the last interglacial, indicating that there was similar ice cover present in the Ross Sea area during MIS 5.5 as during the Holocene.

1 Introduction

Long and detailed climate records obtained from deep ice cores drilled on the East Antarctic ice sheet allow one to assess the past climate variability on various timescales at high southern latitudes (e.g. Petit et al., 1999; EPICA, 2004; Brook et al., 2005; EPICA, 2006; Jouzel et al., 2007). Such climate reconstructions are considered representative for the entire southern high latitude region including Antarctica and the Southern Ocean (SO), the latter playing a crucial role in glacial/interglacial changes and in fast climate changes during the last glacial period (Blunier et al., 1997; Knorr and Lohmann, 2003; Stocker and Johnsen, 2003; EPICA, 2006) as well as in the global carbon cycle (Archer et al., 2000; Toggweiler et al., 2006; Fischer et al., 2010; Bereiter et al., 2012). Despite the wide range of such climate records

from Antarctic ice cores, information on accompanying regional environmental changes is still limited. For example, detailed information on enhanced phytoplankton productivity through atmospheric dust deposition in the SO (iron fertilisation) (Martin, 1990) could contribute to a better understanding of the impact of regional climate changes on the global carbon cycle. Also sea ice in the SO is a key component of the southern high latitude climate system, because an increase in its extent contributes to an increased albedo of the ocean, to a reduced gas exchange, and to decreased ocean mixing (Abram et al., 2013). Sea ice also plays a major role in the formation of deep waters in the ocean, and therefore in global ocean circulation and the carbon cycle (Toggweiler, 1999; Bouttes et al., 2010; Dieckmann and Hellmer, 2010). One possibility to assess past changes in these two parameters are proxy-aerosol records in deep Antarctic ice cores, which provide detailed information on mineral dust deposition and sea ice coverage in different regions of Antarctica (Petit et al., 1990; Röthlisberger et al., 2002; Wolff et al., 2003, 2006; Fischer et al., 2007b; Bigler et al., 2010; Abram et al., 2013).

During glacial/interglacial cycles, most of the variability in atmospheric dust concentration in central East Antarctica was related to the strength of remote continental mineral dust sources and to atmospheric transport efficiency (Fischer et al., 2007b; Petit and Delmonte, 2009). Southern South America (i.e. southern Patagonia) was identified to be the most important source region for glacial terrestrial aerosol transported to East Antarctica (Basile et al., 1997; Gaiero, 2007; Delmonte et al., 2008; Gabrielli et al., 2010; Weber et al., 2012), whereas during the Holocene other remote sources become relatively more important for the dust input to East Antarctica due to the strong decline in dust mobilization in Patagonia (Revel-Rolland et al., 2006; Li et al., 2008; Marino et al., 2009; Gabrielli et al., 2010; Wegner et al., 2012). In addition, dust sources from ice-free areas in the periphery of Antarctica may contribute. While for high-altitude drill sites in the interior of the East Antarctic plateau (e.g. Vostok, EDC) such local sources may be insignificant, their contribution becomes more important for peripheral areas (Bory et al., 2010; Delmonte et al., 2010b; Albani et al., 2012a), in particular those close to the Transantarctic Mountains. The TALDICE (TALos Dome Ice CorE) project provides a deep ice core located at Talos Dome in the Ross Sea sector of East Antarctica in northern Victoria Land (Frezzotti et al., 2007; Stenni et al., 2011). This core is well-positioned to investigate the regional atmospheric circulation changes and their relationship with the glaciation history and environmental changes in the Ross Sea area for the past two glacial/interglacial cycles based on climate proxy as well as terrestrial and sea salt aerosol records.

Physical and chemical properties of dust analysed in Talos Dome snow and ice suggest that local contributions (unconsolidated glacial deposits, for example, in the Antarctic dry valleys and regolith located at high elevation in northern

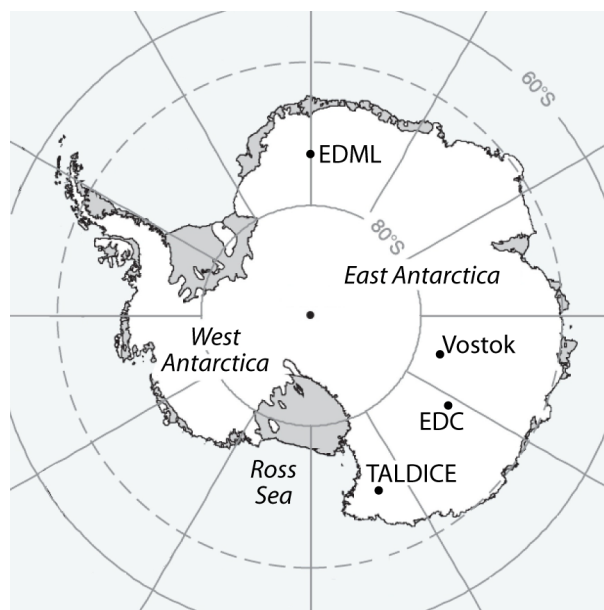


Fig. 1. Map of the Antarctic ice sheet. The four Antarctic drilling sites discussed in this work are indicated. One is located in the Atlantic sector (EDML) and, thus, closer to the southern South American continental dust source than EDC and Vostok, both being located in the Indian Ocean sector. The fourth drilling site, TALDICE, is at a more coastal site close to the Ross Sea and, therefore also influenced by local source regions especially during warm periods.

Victoria Land) to the aeolian dust input was increasing relative to total dust input during the Holocene, when remote sources were low compared to the last glacial period (Delmonte et al., 2010b; Albani et al., 2012a; Delmonte et al., 2013). Dust deflation and transport from proximal sources to the Talos Dome site is influenced by the availability and strength of the dust sources as well as by local meteorological conditions, which in turn are related to regional climate (Albani et al., 2012a). Despite the importance of aeolian dust transport to Antarctica, information on sources and transport of mineral dust from peripheral ice-free areas to the Antarctic interior is still limited. The spatial extent of local dust sources can be assessed by analyses of the isotopic composition of strontium ($^{87}\text{Sr}/^{86}\text{Sr}$) and neodymium ($^{143}\text{Nd}/^{144}\text{Nd}$) in the dust of the ice core samples. However, the extremely low dust concentration in ice cores during interglacial climate conditions makes such analyses extremely difficult (Petit and Delmonte, 2009; Delmonte et al., 2013).

Sea salt aerosol production in coastal Antarctica is related to the presence of sea ice. Brine and frost flower formation (on freshly formed or submerged sea ice) and blowing snow are the most relevant sea salt aerosol sources (Wagenbach et al., 1998; Rankin et al., 2000; Wolff et al., 2003; Yang et al., 2008; Abram et al., 2013). Thus, sea salt aerosol input on the East Antarctic plateau should be linked at least in part to the sea ice extent in the SO. Accordingly, sea salt aerosol

Table 1. Geographical and glaciological setting of the drill sites. Modern altitude is given in m a.s.l. (above sea level), average Holocene accumulation rates are given in ($\text{kg m}^{-2} \text{a}^{-1}$).

| | TALDICE | EDC | EDML | Vostok |
|--------------------------|---------------------|---------------------|--------------------|---------------------|
| Geographic location | 72°70' S, 159°11' E | 75°06' S, 123°21' E | 75°00' S, 00°04' E | 78°28' S, 106°50' E |
| Altitude (m a.s.l.) | 2319 | 3233 | 2882 | 3488 |
| Modern accumulation rate | 73 | 26 | 55 | 24 |

source regions for the Atlantic and Indian Ocean sector of Antarctica are spatially not the same and source strength as well as transport may have changed independently in different regions around Antarctica. Accordingly, we interpret sea salt sodium as a sea ice proxy restricted to the adjacent ocean source areas, which are the Atlantic Ocean sector of the SO for EDML, the Indian Ocean sector for EDC and Vostok, and the Ross Sea sector for TALDICE, as indicated by back trajectory calculations (Reijmer et al., 2002; Scarchilli et al., 2011) and by the limited atmospheric lifetime of the sea salt aerosol (Fischer et al., 2007b; Röthlisberger et al., 2010).

In this study we report on mineral dust represented by non-sea salt calcium (nssCa^{2+}) and sea salt aerosol represented by sea salt sodium (ssNa^+) records from TALDICE in centennial resolution reaching back 150 thousand years before present (ka BP), where present refers to 1950 AD. The new proxy data from TALDICE based on continuous flow analysis (CFA) techniques is compared to three other East Antarctic ice core records in the following, all covering at least the last 150 ka (a map of Antarctica with all investigated ice core sites is shown in Fig. 1; Table 1 provides further information about the sites). These are the two deep ice cores drilled within the European Project for Ice Coring in Antarctica (EPICA) at Dome C (EDC) (EPICA, 2004) and at Kohnen station in Dronning Maud Land (EDML) (EPICA, 2006), as well as the Vostok ice core (Petit et al., 1999). Fischer et al. (2007a) have already shown that a comparison of nssCa^{2+} records of different ice cores can reveal substantial information about the sources and transport mechanisms of dust deposited on the East Antarctic plateau. Here we extend the findings by Fischer et al. (2007a) with a multi-site comparison of nssCa^{2+} ice core records in centennial resolution, complemented with model data of dust deposition on the East Antarctic plateau available for the Last Glacial Maximum (LGM) and the Holocene. In addition, the ssNa^+ records of the different drill sites give indications on the evolution of local sea ice coverage in the Atlantic Ocean, Indian Ocean, and Ross Sea sector of the SO during the past 150 ka BP.

2 Materials and methods

2.1 Data acquisition and performance

This study is based on high-resolution calcium (Ca^{2+}) and sodium (Na^+) CFA data from the Antarctic ice cores EDC (Röthlisberger et al., 2004; Bigler et al., 2006, 2010), EDML (Ca^{2+} CFA data have already been discussed in Kaufmann et al., 2010; Na^+ CFA data represent new data), and TALDICE (new data). All analyses were performed using CFA (Röthlisberger et al., 2000; Kaufmann et al., 2008), providing aerosol chemistry data in unprecedented resolution and avoiding analytical blank issues, which are especially important in the case of Ca^{2+} (Fischer et al., 2007a; Kaufmann et al., 2010). Besides these high-resolution data, we included Na^+ and Ca^{2+} records from the Vostok ice core in our multi-site comparison, which are available in coarse resolution only (De Angelis et al., 1997) and are based on discrete ion chromatographic (IC) analysis of samples after manual decontamination.

CFA measurements of TALDICE were performed in the years 2006–2008 at the Alfred-Wegener-Institut (AWI) in Bremerhaven, Germany. The covered depth interval (305–1435 m) corresponds to an age interval of 3.8–150 ka BP. Major gaps in the new TALDICE data sets can be found in the Ca^{2+} record from 490–502 m and from 535–578 m, as well as in the Na^+ record from 441–449 m, respectively. Apart from the mentioned gaps, no gaps longer than five consecutive metres can be found in either of the new records (see Fig. 2). The longer gaps are due to maintenance and failure of the respective CFA detector, while measurements were continued. Other smaller gaps are mainly due to bad ice quality (mostly in the brittle ice zone) or distinct visible (ash) layers which were not processed with CFA. Apart from these gaps, continuous records have been achieved with a sampling resolution of 0.5 cm or better.

Due to signal dispersion in the CFA system the effective depth resolution is 1 cm (Ca^{2+}) and 2 cm (Na^+) at a melt speed of approx. 4 cm min^{-1} as it was applied during the TALDICE analyses (Kaufmann et al., 2008). Limit of detections (LOD) are 0.1 ppbw for Ca^{2+} and 0.5 ppbw for Na^+ , respectively, measurement errors are estimated to be generally below 10 % (Röthlisberger et al., 2000; Kaufmann et al., 2008). The sample decontamination accomplished by continuously melting the ice core samples during CFA

measurements reduces process blanks considerably compared to manual ice sample decontamination for IC measurements. As a consequence, the LOD of CFA are significantly lower compared to IC measurements.

EDML Na^+ data in the age interval 123.3–132.3 ka BP (depth: 2341–2383 m) have been analysed using IC (Fischer et al., 2007a) in 1 m resolution due to missing CFA Na^+ data in this depth interval. On the Vostok ice core 237 discontinuous measurements have been analysed with a mean depth resolution of 10.1 m using IC only (De Angelis et al., 1997). Each individual Vostok ice sample (once decontaminated by rinsing) was generally 10 cm long. Of these measurements, covering a depth range of 100–2500 m, we show 218 data points which represent the age range 5–150 ka BP, resulting in a mean age resolution of 665 yr.

2.2 Data treatment and dating

In order to compare the different ice cores, the different resolutions of the data sets have to be considered. Therefore, equidistant age averages (100 and 500 yr for all the high-resolution records, and 500 yr only for the Vostok records) were calculated for all four ice cores using the well-synchronised recent AICC2012 age scales (Bazin et al., 2013; Veres et al., 2013). In the following we describe how this is achieved based on the three high-resolution records and the discrete IC records of Vostok ice core.

The age scale (given in 1–3 m resolution, depending on the ice core and depth range) has been interpolated to assign an age to each individual data point of the high-resolution records. In the same way the accumulation rates have been interpolated in order to calculate deposition fluxes and to reconstruct the atmospheric signals (see next section). Centennial medians have then been calculated from the high-resolution data on the common age scale for each record. Medians have been calculated to prevent the hundred year mean values from being biased by single extreme events. The number of high-resolution data points per 100 yr interval ranges from 6000 (Holocene) to 77 (during the penultimate glacial, i.e. 140 ka BP) due to the increasing thinning of the ice layers towards the bottom. If more than two thirds of the high-resolution data within the interval, from which a 100 yr median has been calculated, were missing, the median has been discarded, again in order to prevent an extreme event to bias the result significantly. The same threshold has been applied for the calculation of the 500 yr medians. With this threshold we discarded up to 7 % of the calculated data of a single record.

For the Vostok records, available in coarser resolution only, we simply interpolated the age scale to assign an age to each data point at its individual depth. From these data points we then interpolated Na^+ and Ca^{2+} concentrations to obtain a value for each 500 yr step in accordance with the 500 yr means of the three other cores. No 100 yr values have been calculated for Vostok due to the coarse resolution of

the original data sets. We acknowledge that this is an inaccurate treatment from a statistical point of view. However, the records we obtain in this way are used for illustrative purpose only, while the significance is in no way comparable to the records of the other three cores.

2.3 Crustal, sea salt, and flux correction

In addition to water-insoluble mineral dust particles, also water-soluble Ca^{2+} ions can be considered as a valuable ice core proxy of continental aerosol input onto the East Antarctic ice sheet. However, not only continental sources emit Ca^{2+} but also sea water can have a considerable contribution to the total Ca^{2+} load in the air masses, especially during interglacial periods. Sodium on the other hand originates mainly from the marine source, but has some continental source contribution as well. Thus, the sea water contribution has to be subtracted from the total Ca^{2+} signal in order to obtain the nssCa^{2+} concentration representing continental dust input. On the other hand, the continental contribution has to be subtracted from total Na^+ in order to obtain the ssNa^+ signal only. In all four ice core records the nssCa^{2+} and the ssNa^+ fractions, respectively, are calculated from the Ca^{2+} and Na^+ records according to Bigler et al. (2006), using an empirical Antarctic ice core specific crustal correction for Ca^{2+} and Na^+ , respectively.

Calcium and sodium are both conservatively deposited onto the ice sheet, thus there is no need to account for additional post-depositional effects distorting the signals in the ice.

In order to account for the dilution of the original atmospheric aerosol concentrations in the ice core samples by snow accumulation, the measured concentrations have to be corrected for this effect. This is achieved by multiplying the measured concentrations by the modelled accumulation rate at the respective depth or age, resulting in the total deposition flux of the aerosol (Wolff et al., 2006; Fischer et al., 2007b). For EDC, EDML, and Vostok atmospheric aerosol concentrations have been reconstructed by multiplying the ssNa^+ and nssCa^{2+} concentration records with the accumulation rate given by the AICC2012 age scale. For TALDICE we have used the accumulation rate calculated by Buiron et al. (2011), which has also been used for modelling the AICC2012 timescale of TALDICE. All age scales, and thus accumulation rates, use the inverse model by Lemieux-Dudon et al. (2012). The accumulation rates are typically given in 1–3 m resolution, corresponding to a few years or a few hundred years depending on the depth range. In low accumulation sites, where the total deposition flux of an aerosol is dominated by dry deposition, the flux is essentially independent of changes in the accumulation rate and thus almost proportional to the original atmospheric aerosol concentration (Fischer et al., 2007b). Therefore, we discuss aerosol fluxes in this study, which are more representative of the original atmospheric aerosol concentrations. It is acknowledged

that in contrast to EDC and Vostok, where dry deposition is predominant, EDML and Talos Dome are more intermediate accumulation sites (see Table 1 for average Holocene accumulation rates). Thus, wet deposition can have a significant influence on the deposition fluxes, potentially introducing additional variations in the calculated flux rates of EDML and TALDICE data used in this work. Furthermore, the uncertainties of the modelled accumulation rates are usually around 20 %. Together with the estimated concentration errors, which are below 10 %, the uncertainties of the total deposition fluxes are estimated to be smaller than 30 %. Even though this estimated error is considerable, it is small compared to glacial/interglacial nssCa^{2+} flux changes, which are of the order of one magnitude.

2.4 Model for aerosol transport

In order to discuss our proxy-aerosol data and compare them with other East Antarctic ice core records, we applied a simple exponential transport model which is presented in the following. Assuming a simple model of atmospheric aerosol transport as described by Fischer et al. (2007a) with an aerosol concentration $C_{\text{air}}(0)$ at the source and an exponential loss during transport, the concentration of the aerosol in the air parcel at any time t can be described as

$$C_{\text{air}}(t) = C_{\text{air}}(0) \cdot \exp(-t/\tau),$$

where τ is the average atmospheric residence time of the aerosol. Using this simple transport model and assuming a single source region (e.g. Patagonia), the logarithmic air concentration of the aerosol at one site (e.g. EDC) with transport time t_2 from the source location to the site can be expressed by the concentration at another site (e.g. EDML) with transport time t_1 according to

$$\ln [C_{\text{air}}(t_2)] = \ln [C_{\text{air}}(t_1)] - \Delta t/\tau,$$

where $\Delta t = t_2 - t_1$ is the difference of the transport times from the source to the two sites, assuming that the atmospheric residence time along the two transport ways is the same. Thus the relation of the logarithms of the atmospheric aerosol concentration at the two drilling sites is linear to first order with an offset $\Delta t/\tau$.

3 Results and discussion

3.1 The main features of the new TALDICE non-sea salt calcium and sea salt sodium records

In this publication we present the first continuous high-resolution records of Ca^{2+} and Na^+ of the Talos Dome ice core. The concentrations of the two species are shown in Fig. 2 versus depth in 10 cm and 1 m resolution along with the TALDICE $\delta^{18}\text{O}$ profile in 1 m resolution (Stenni et al.,

2011) and the age scale derived accumulation rate at Talos Dome. Since part of the concentration changes seen in Fig. 2 are simply due to the fact that the snow accumulation rate is changing considerably (more than a factor of two, see 2nd panel in Fig. 2) over glacial/interglacial cycles, we will discuss the fluxes of the source separated signals in the following.

The different East Antarctic nssCa^{2+} flux records are discussed and compared in Sect. 3.3 and Sect. 3.4. While the fluxes of EDC and EDML evolved synchronously during the past 150 ka with a constant offset, the TALDICE nssCa^{2+} flux seems to oscillate between the other two records. Interestingly, TALDICE values are following the EDC flux during cold periods, while during warmer periods (grey shaded panels in Fig. 3) they are considerably higher than in EDC. This observation is discussed in Sect. 3.4.2, while in Sect. 3.4.1 nssCa^{2+} fluxes of EDC and EDML are compared in more detail. In the following section (Sect. 3.2) ssNa^+ flux is discussed and compared with the EDC and EDML records over the past 150 ka.

3.2 Sea salt sodium

3.2.1 The last glacial period

During cold periods the sea salt flux is rather constant in all three ice cores compared to coeval ice extent changes inferred from marine sediment data. The sea salt flux in ice cores appears to be increasingly insensitive for very large sea ice extents as a result of the vast source area available, when the sea ice around Antarctica extends further north. Additionally, the distance from the sea ice margin to the drill sites on the ice sheet is increasing and, thus, the travel time from the source to the deposition area is increasing significantly compared to the atmospheric lifetime of sea salt aerosol (Fischer et al., 2007b; Röthlisberger et al., 2010; Abram et al., 2013). Thus, ssNa^+ in ice cores provides a tool for qualitative investigations on sea ice extent during cold periods, however, quantitative interpretations are hampered by this effect.

In the period 115–20 ka BP TALDICE ssNa^+ flux is mostly lower than in EDML (bottom panel in Fig. 3). Only during two periods, each about ten thousand years long (40–30 ka BP and 65–55 ka BP, respectively), the sea salt aerosol input is higher in TALDICE. From 40–30 ka BP, including Antarctic isotope maxima (AIM) 8–4 (EPICA, 2006), $\delta^{18}\text{O}$ is higher at EDML compared to TALDICE (see Fig. 3, top panel). This could indicate moderately elevated temperatures in the Atlantic sector possibly causing a decrease in sea ice extent in this region with a consequent impact on the ssNa^+ signal in EDML. Remarkably, EDML ssNa^+ flux in this period is the lowest observed during the entire last glacial period. During the other period, 65–55 ka BP, marking the transition from MIS 4 into MIS 3, rather high TALDICE values instead of particularly low EDML values are responsible for the inversion of the flux relationship. This high sea

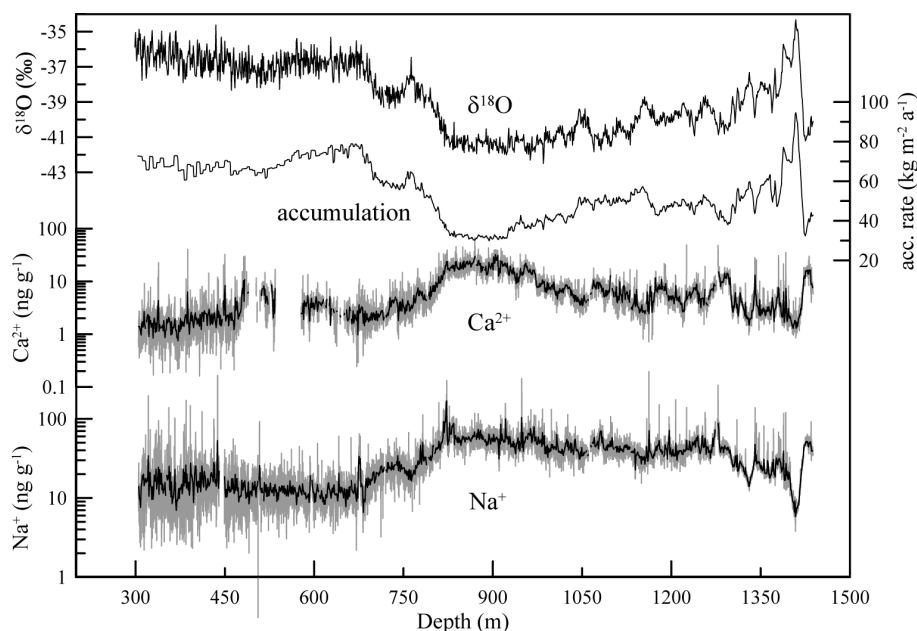


Fig. 2. The $\delta^{18}\text{O}_{\text{ice}}$ profile of TALDICE (Stenni et al., 2011) is shown in the top panel. In the second panel the accumulation rate is shown as modelled in the recent AICC2012 age scale for Talos Dome (Bazin et al., 2013; Veres et al., 2013). The third and fourth panels show TALDICE Ca^{2+} and Na^{+} concentrations, respectively (new CFA data); note the logarithmic scale for both records. Black lines indicate 1 m mean values, grey lines indicate 10 cm mean values, both calculated from the high-resolution CFA data. All data are plotted versus depth along the Talos Dome ice core.

salt aerosol input in TALDICE is accompanied by large flux variations and marks a transition from low/moderate ssNa^{+} fluxes during MIS 5.4–MIS 4 (115–60 ka BP) to high fluxes during MIS 3 (60–25 ka BP); in fact the mean flux is increasing by a factor of 1.5. In contrast to Talos Dome such a shift in the mean ssNa^{+} fluxes cannot be observed in EDC or EDML. There are indeed some distinct long-term ssNa^{+} flux changes in both records, however, the variations remain around the same mean values for the entire last glacial period. Accordingly, the TALDICE record points to a shift in sea ice coverage in the Ross Sea sector from MIS 5 to MIS 3, which appears to be less pronounced in the Atlantic or Indian Ocean sector as reflected in the EDML and EDC core, respectively. In contrast, at those two sites, a stronger shift in sea ice coverage is indicated during full interglacials compared to TALDICE, with the warmer MIS 5.5 showing even a substantially smaller sea ice extent compared to the Holocene.

3.2.2 Holocene versus last interglacial

When comparing the ssNa^{+} flux of the Holocene with marine isotope stage (MIS) 5.5, it becomes evident that the same level is reached in TALDICE for both interglacials, while for EDC and EDML fluxes during MIS 5.5 were only half (EDC) or even less (EDML) of the Holocene levels (see Fig. 3). EDC ssNa^{+} flux is strongly related to winter sea ice extent in the Indian Ocean sector of the SO (Wolff et al., 2006) due to very low summer sea ice extent in this area

even during glacial periods (Gersonde et al., 2005). However, EDML ssNa^{+} flux during MIS 5.5 is even more reduced than in EDC, possibly due to an even stronger decline in sea ice coverage in the Atlantic sector related to a reduction of both winter and summer sea extent in the Atlantic sector at that time (Gersonde et al., 2005; Fischer et al., 2007a). The very low ssNa^{+} fluxes of EDC and EDML are in line with warmer Antarctic temperatures during MIS 5.5 compared to the Holocene (EPICA, 2006), causing significantly lower sea ice extent during that period. However, TALDICE ssNa^{+} flux is at about the same level during both interglacial periods. This indicates that substantial parts of the ssNa^{+} source regions for Talos Dome remain active during MIS 5.5, which excludes the Indian Ocean sector as a major ssNa^{+} source region for Talos Dome, because this is the main source region for EDC where a drastic reduction of ssNa^{+} input can be observed. Based on these observations we suggest that a major part of sea salt aerosol input to Talos Dome is originating from the Ross Sea sector not only during the Holocene but also during MIS 5.5. This consequently implies that a significant part of the sea ice cover in the Ross Sea embayment was persistent also during MIS 5.5 and was an active source for Talos Dome ssNa^{+} input. This may be also of glaciological interest because the existence and/or extension of the Ross ice shelf during the warm MIS 5.5 period is controversial up to now (e.g. McKay et al., 2012). Based on marine sediments in the Ross Sea embayment McKay et al. (2012) find that the marine ice sheet in the western Ross Embayment has

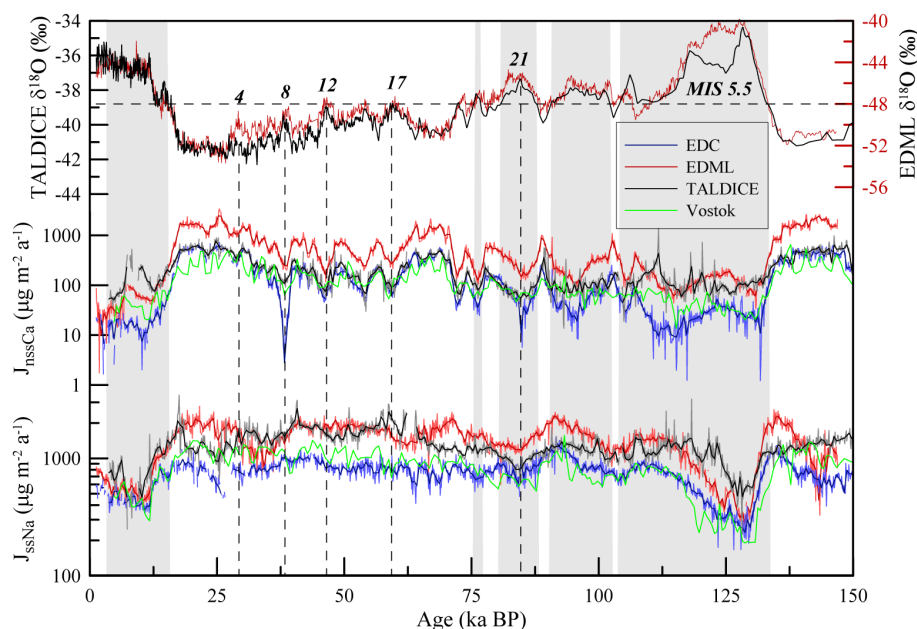


Fig. 3. Top panel: the $\delta^{18}\text{O}_{\text{ice}}$ profile of TALDICE (Stenni et al., 2011) and EDML (EPICA, 2006) are shown to illustrate the temperature evolution at the two drill sites. The dashed horizontal line indicates the TALDICE temperature threshold ($\delta^{18}\text{O}_{\text{ice}} = -38.9\text{‰}$) used to discriminate warm and cold periods, (see text for explanation). Accordingly, the grey shadowed areas indicate warm periods ($\delta^{18}\text{O}_{\text{ice}}$ above threshold). Major AIM events (EPICA, 2006) are indicated by numbers above the curve, the dashed vertical lines indicate the maxima of the corresponding AIM events. Middle panel: the nssCa^{2+} flux (J_{nssCa}) of TALDICE (new CFA data) is plotted in black along the one of EDC (blue) (Bigler et al., 2006), EDML (red) (Kaufmann et al., 2010), and Vostok (green) (De Angelis et al., 1997). Bottom panel: the ssNa^{+} flux (J_{ssNa}) of TALDICE (new data) is plotted in black along the one of EDC (blue) (Bigler et al., 2006), EDML (red, new CFA data), and Vostok (green) (De Angelis et al., 1997). Light colours indicate 100 yr median values, dark colours 500 yr median values. All data are shown on the AICC2012 age scale.

oscillated between a grounded ice sheet and floating ice shelf at least seven times during the past 800 ka. Interglacials during this period in the Ross Sea were probably characterised by ice shelf conditions similar to, or more extensive than those of the present day. Open/proximal marine conditions may have occurred in the Ross Island region during MIS 5.5 or 7, or potentially both (McKay et al., 2012, and references therein).

3.3 Non-sea salt calcium

3.3.1 The last 20 000 yr

In the middle panel of Fig. 3 nssCa^{2+} flux is plotted for the past 150 ka. Distinct changes in the flux rates can be observed along with major changes in temperature (top panel in Fig. 3). However, it can be seen that these flux rate changes are much less pronounced in TALDICE than in the other cores. This is most evident for nssCa^{2+} fluxes during glacial/interglacial transitions where flux rate changes of a factor of four are prevailing for TALDICE (see Table 2). As a comparison, the glacial/interglacial flux rate changes are of the order of a factor of 20 for EDC and EDML. The rather high Holocene values in TALDICE are in line with previous results of dust and iron (Fe) fluxes (Albani et al., 2012a; Val-

lelonga et al., 2013), and also show a comparable temporal evolution. After a minimum at around 12–13 ka BP during the Antarctic cold reversal, the nssCa^{2+} flux increases again during the early Holocene in the TALDICE record. The flux values show a maximum at about 8 ka BP after which they decrease continuously (see Fig. 4). During the Holocene the other two cores, especially EDML, show a similar behaviour, however, at a much lower level and with much less distinct flux rate changes compared to TALDICE.

This behaviour might point to additional dust sources proximal to the TALDICE drill site becoming available at the beginning of the Holocene, e.g. from glacial drift left behind from retreating glaciers during the retreat of the Ross ice shelf between 13 and 9 ka BP. Afterwards, the efficient new sources might get more and more depleted, leading to a steady decrease of dust input from these sources during the mid-Holocene. Such a steady depletion of the local dust source would be expected to be accompanied by a coeval shift within the dust grain size distribution (i.e. an increasing contribution of smaller particles). However such behaviour is not corroborated by dust particle size distributions as pointed out by Albani et al. (2012a), who report variable rather than constant dust grain size distribution after the deglaciation. Instead, they suggest that the retreat of the Ross ice shelf

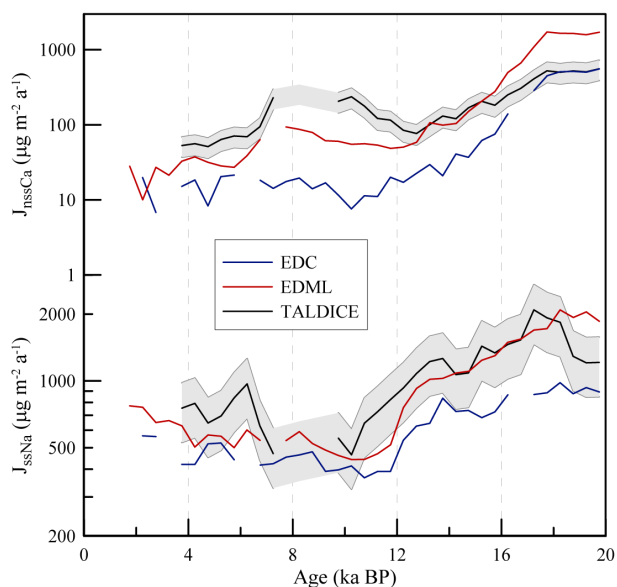


Fig. 4. NssCa^{2+} (J_{nssCa}) and ssNa^{+} (J_{ssNa}) fluxes for the Holocene and T1. The grey shaded bands indicate the range covered by the estimated 30 % error as mentioned in Sect. 2.3. In TALDICE, they show opposite trends during the deglaciation and early–mid-Holocene (i.e. 13–6 ka BP).

≈ 8 ka BP and the coeval opening of the Ross Sea embayment could have caused a modification of the regional atmospheric circulation patterns.

The distribution of air mass trajectories after 8 ka BP was less favourable for the transport of local dust to the TALDICE site, since those trajectories passing over the Ross Sea became relatively more frequent (Albani et al., 2012a). As a consequence, dust and nssCa^{2+} fluxes in TALDICE are expected to decrease as it is indeed observed in both records. In addition, simultaneously elevated ssNa^{+} input would be expected due to an increased frequency of air masses passing over the Ross Sea. Looking at Fig. 4 it becomes evident that the decrease in nssCa^{2+} after 8 ka BP is coeval with a significant increase in ssNa^{+} in the TALDICE record. In fact, the fluxes of nssCa^{2+} and ssNa^{+} show opposing trends during the early Holocene. While both fluxes start decreasing at the beginning of the deglaciation at ≈ 18 ka BP, nssCa^{2+} increases again after 12 ka BP to reach a local maximum at about 8 ka BP (upper panel in Fig. 4). The flux of ssNa^{+} on the other hand is continuously decreasing until it reaches a local minimum at around 8 ka BP (lower panel in Fig. 4). This indicates that indeed air mass provenance is likely to be responsible for Holocene dust and sea salt aerosol input changes at TALDICE, in addition to new local dust sources available during warm periods. In summary, based on our ssNa^{+} and nssCa^{2+} records we can corroborate the findings of Albani et al. (2012a), suggesting that more frequent air mass trajectories through the Ross Sea after 8 ka are mainly

responsible for a reduced dust input from local sources after the Holocene maximum around 8 ka BP.

3.3.2 The effect of dust deposition in the Southern Ocean to deglacial CO_2 changes

It is evident that during glacial conditions nssCa^{2+} fluxes are strongly related to temperature in all four ice cores, albeit not linearly (see Fig. 3, note logarithmic axis for nssCa^{2+}). In particular, it can be seen that nssCa^{2+} decreases significantly during each of the major AIM (EPICA, 2006), suggesting synchronous changes in the southern South American source regions during warmer climate conditions of the last glacial (Wolff et al., 2006). It can also be observed that the nssCa^{2+} flux at EDC shows a very constant offset to EDML throughout the entire period shown in Fig. 3.

During AIM 8 (approx. 40 ka BP) EDC the nssCa^{2+} flux shows a distinct dip with values reaching down to low interglacial level. These extreme low values are reached neither in the EDML nor in the TALDICE nor in the Vostok data during AIM 8. Even in the EDC record of insoluble dust particles (Lambert et al., 2008), which is otherwise strongly correlated to nssCa^{2+} , the AIM 8 minimum is not as pronounced as in the nssCa^{2+} record, nor is it in the EDC nssCa^{2+} data measured by ion chromatography (Wolff et al., 2006). Bigler et al. (2010) mentioned some distorted CFA Ca^{2+} measurements due to occasional baseline fluctuations in the depth interval 585–788 m, comprising particularly AIM 8. Thus, EDC nssCa^{2+} CFA data in the age interval 37.5–39 ka BP appear to be affected by analytical issues and are not included in the further discussion and are marked specifically in Fig. 6 (see figure caption for details).

Due to the refusal of the extreme low EDC nssCa^{2+} values during AIM 8, we briefly revise the effect of aeolian dust deposition in the SO (and thus iron fertilisation) to atmospheric CO_2 changes as previously discussed by Röthlisberger et al. (2004). Based on our new data, which allow for the calculation of an East Antarctic composite nssCa^{2+} flux record, we conclude that the upper limit of a 20 parts per million (ppm) contribution of changes of Fe supply to the SO to the total increase of 80–100 ppm CO_2 during the last glacial termination (T1), as suggested by Röthlisberger et al. (2004), is too low. Their calculations are relying strongly on the low nssCa^{2+} flux values during AIM 8 in EDC, which biases the estimated influence of reduced iron fertilisation to the CO_2 increase.

Based on Fe records of EDC and Talos Dome, Vallelonga et al. (2013) estimated the impact of iron fertilisation through additional Fe input to the SO during the transition from MIS 3 into the LGM on atmospheric CO_2 to be of the order of 20 ppm. However, this is an estimate restricted to MIS 3/LGM only and, thus, this value cannot be directly compared to the influence of the much stronger Fe input changes on the atmospheric CO_2 increase during T1 as discussed here. There have been other studies based on ice

Table 2. Transport model results and ice core averages. In the first row the $\Delta t/\tau$ values of EDML vs. EDC for different time periods during the past 150 ka are shown. Below, the fluxes of nssCa^{2+} (J_{nssCa}) and ssNa^+ (J_{ssNa}) are indicated for EDC, EDML, and TALDICE, for the corresponding time intervals (given in $\mu\text{g m}^{-2} \text{a}^{-1}$).

| Time period (ka BP) | Holocene 3–15 | LGM 15–30 | MIS 3 30–60 | MIS 4–5.4 60–115 | MIS 5.5 115–133 | MIS 6 133–146 |
|-------------------------------------|------------------|-----------------|-----------------|---------------------|--------------------|------------------|
| $\Delta t/\tau_{(\text{EDML/EDC})}$ | 1.22 ± 0.61 | 1.19 ± 0.16 | 1.40 ± 0.43 | 1.48 ± 0.39 | 1.54 ± 0.57 | 1.38 ± 0.30 |
| EDC | | | | | | |
| J_{nssCa} | 22 ± 14 | 414 ± 145 | 141 ± 84 | 118 ± 121 | 30 ± 17 | 384 ± 113 |
| J_{ssNa} | 515 ± 134 | 786 ± 142 | 866 ± 112 | 830 ± 161 | 455 ± 187 | 816 ± 205 |
| EDML | | | | | | |
| J_{nssCa} | 76 ± 49 | 1433 ± 505 | 555 ± 277 | 442 ± 396 | 130 ± 56 | 1559 ± 519 |
| J_{ssNa} | 684 ± 245 | 1802 ± 332 | 1656 ± 334 | 1536 ± 310 | 761 ± 417 | 1454 ± 512 |
| TALDICE | | | | | | |
| J_{nssCa} | 136 ± 86 | 507 ± 138 | 190 ± 93 | 170 ± 138 | 110 ± 68 | 422 ± 132 |
| J_{ssNa} | 850 ± 309 | 1336 ± 383 | 1750 ± 323 | 1223 ± 293 | 969 ± 364 | 1279 ± 158 |

core Fe measurements investigating T1 (Gaspari et al., 2006; Spolaor et al., 2013) which conclude that a reduction in iron fertilisation in the SO contributed up to 40 ppm to the CO_2 increase during T1. Also an estimate based on Fe measurements in marine sediments constrains the effect of natural aeolian iron deposition on marine export production in the SO region to up to 40 ppm of the atmospheric CO_2 concentration changes during the last glacial cycle (Martínez-García et al., 2011).

In order to calculate the spatially most representative record of dust deposition changes in the Antarctic/SO region, we calculated a composite of the EDC, EDML, and TALDICE nssCa^{2+} records. Our composite nssCa^{2+} flux record uses the arithmetic average, however, with some exceptions described in the following. EDML values were corrected for their offset compared to EDC and TALDICE. This was done by matching the logarithmic EDML values to those of EDC during the LGM (24–19 ka BP) when the common southern South American source was strongest, and then linearly shifting the entire EDML record according to the resulting offset. TALDICE values younger than 15 ka BP were discarded for the calculation because of their higher Holocene values compared to EDC and EDML reflecting the substantial contribution of local sources. During AIM 8 (A1) (i.e. 39.3–37.4 ka BP), the EDC values were discarded (see Fig. 5a). In Fig. 5b the linear regression of the composite nssCa^{2+} flux vs. atmospheric CO_2 is shown for T1 and for the period covering A1–A4 as done by Röthlisberger et al. (2004). Due to the omission of the low EDC nssCa^{2+} flux during AIM 8, our regression through the points covering A1–A4 is much steeper compared to the one obtained by Röthlisberger et al. (2004). Following the argumentation of Röthlisberger et al. (2004), we conclude that the reduction of iron supply through reduced aeolian dust deposition over the SO may have contributed up to 40 ppm to the at-

mospheric CO_2 increase during T1, which is in line with the results based on ice core Fe analyses of Gaspari et al. (2006).

3.4 Non-sea salt calcium and sea salt sodium during the last 150 000 years

3.4.1 Comparison of EDC versus EDML

In the following we compare different nssCa^{2+} records using our simple exponential transport model as described in Sect. 2.4. In this section we update a comparison study between EDC and EDML done by Fischer et al. (2007a), while in the next section (Sect. 3.4.2) the comparison is extended to Vostok and the new TALDICE nssCa^{2+} record.

In Fig. 6 the logarithms of nssCa^{2+} and ssNa^+ fluxes are plotted for all three ice cores versus each other. In the first panel of Fig. 6a fluxes of EDC are plotted versus those of EDML, as has been done previously by Fischer et al. (2007a) with the only difference that we use CFA data. In contrast, Fischer et al. (2007a) analysed the EDML ice core samples by IC with a significant blank contribution in the Ca^{2+} data leading to an offset during warm (low concentration) periods. To illustrate this problem we plotted the EDML data analysed by IC vs. EDC data in Fig. 6f with the only difference, compared to Fischer et al. (2007a), being that we used the AICC2012 age scale with its respective accumulation rate. In light green, all data are shown, in dark green the data with original Ca^{2+} concentrations higher than 7 ppb, assuming that only data below this threshold are significantly biased by the blank contribution. A subsequent comparison of the linear regressions through all the IC data (slope a of the regression is 1.26) and those above the threshold only ($a = 1.13$) show that the IC data set is indeed approaching the slope of the CFA data set ($a = 1.02$) when low concentration IC values are excluded. This procedure does not exclude the contaminated Ca^{2+} data which exceed the threshold of 7 ppb

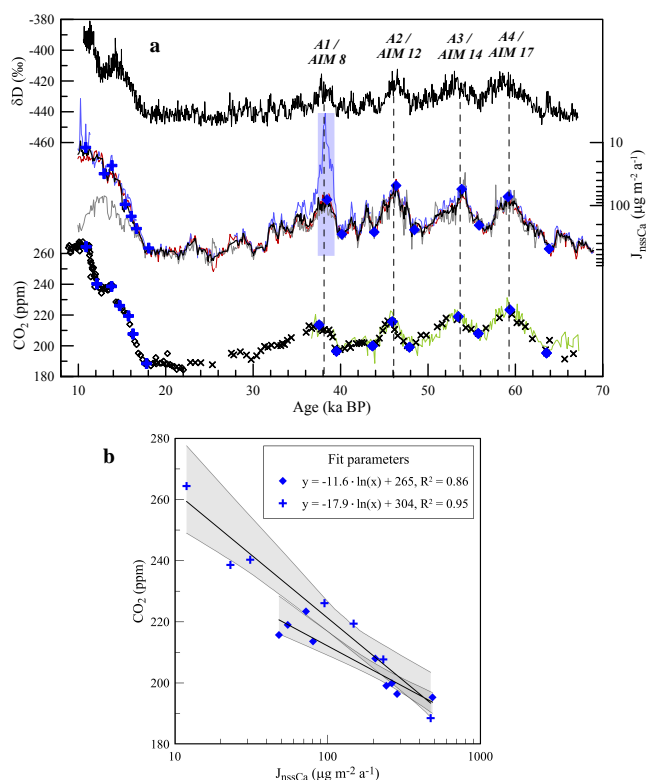


Fig. 5. (a) Estimate of CO_2 sensitivity on dust changes. EDC δD is shown in the top panel, CO_2 concentrations from EDC (black open diamonds) and Taylor Dome (black crosses) in the bottom panel. More recent EDML and TALDICE CO_2 concentrations (Bereiter et al., 2012) are shown for comparison (green line). The middle panel shows the mean $nssCa^{2+}$ flux (J_{nssCa}) calculated from the 100 yr medians of EDC, EDML, and TALDICE (black line); discarded EDC values during AIM 8 are marked by the blue shaded area. Blue diamonds and crosses in the bottom panel indicate the same tie points used for the linear regression calculation as done by Röthlisberger et al. (2004). In addition, the 100 yr means of EDC (blue line), offset-corrected EDML (red line), and TALDICE (grey line) are shown in the middle panel. (b) Linear regressions of the blue diamonds and crosses from (a), according to Röthlisberger et al. (2004). Due to the discarded EDC values during AIM 8 we obtain a regression line of the diamonds (representing CO_2 and $nssCa^{2+}$ during A4–A1) much closer to the one during T1, indicated by the crosses. Grey shaded areas indicate the 95 % significance intervals.

and is therefore not providing a thorough correction, nevertheless, it is seen that the IC blank contribution has a significant effect, which biases the outcome of the investigations as already mentioned in Fischer et al. (2007a). Furthermore, if only data of the cold periods are investigated, the two data sets (IC and CFA $nssCa^{2+}$) are in accordance with each other, resulting in the same linear regressions of the two plots (not shown).

When using CFA data it can only be seen that the offset $\Delta t/\tau$ has been constant over the whole period. The linear

fit through all data points reveals a slope of $a = 1.02$ with $r^2 = 0.87$ (total number of data points $N = 1336$). The offset $\Delta t/\tau$ during the Holocene is 1.22 ± 0.65 , during the LGM is it 1.19 ± 0.16 , thus virtually the same. This is remarkable, since different glacial/interglacial variations in dust and other aerosol input have often been attributed to changes in wind speed and atmospheric circulation around Antarctica and, thus, to transport effects (e.g. Petit et al., 1990, 1999). Indeed there have been more recent studies, which suggest only moderate glacial/interglacial variations in wind speed and latitudinal shifts of the westerlies based on atmospheric circulation models (Krinner and Genthon, 1998, 2003; Mahowald et al., 2006; Sime et al., 2013) as well as based on size distribution measurements of particulate dust in East Antarctic ice cores (Delmonte et al., 2004).

Based on our simple transport model, we cannot see any transport effects influencing atmospheric dust concentrations at the two drilling sites during the last 150 ka. Yet, changing wind speeds (i.e. more efficient transport for colder climate conditions) could still be compensated by simultaneous changes of τ . However, this would require decreased atmospheric residence times during colder periods, although τ is suggested to be longer during colder conditions due to reduced wet deposition en route (Yung et al., 1996; Petit et al., 1999; Lambert et al., 2008). Other studies highlight the spatially variable nature of dust lifetimes, which depend on the transport pathways (Albani et al., 2012b). In summary, based on our multi-site $nssCa^{2+}$ flux records we conclude that transport intensity as well as atmospheric residence time plays a minor role for the observed dust flux changes on the East Antarctic plateau during the last two glacial/interglacial cycles. Instead, our transport model suggests source strength changes to be mainly responsible for the pronounced $nssCa^{2+}$ changes (EDC and EDML $nssCa^{2+}$ flux ratio LGM/Holocene ≈ 18 , see Table 2) on the East Antarctic plateau as suggested by previous studies (e.g. Wolff et al., 2006; Fischer et al., 2007a).

Southern South America is believed to be the most important source region for glacial terrestrial aerosol to East Antarctica (Basile et al., 1997; Gaiero, 2007; Delmonte et al., 2008), whereas during warmer periods also Australia or other remote source regions become relatively more important (Revel-Rolland et al., 2006; Li et al., 2008; Marino et al., 2009; Gabrielli et al., 2010; Albani et al., 2012b). Based on the transport model applied in our study, several source regions with considerable geographic distance can not be excluded. However, this would require similar $\Delta t/\tau$ values for all contributing sources or a constant source mix with different $\Delta t/\tau$ over time for each contributing source to obtain a linear relation between EDC and EDML $nssCa^{2+}$ fluxes as shown in Fig. 6a. The variability of $nssCa^{2+}$ fluxes increases slightly for lower concentrations (Fig. 6a), thus for warmer climate conditions, which might be attributed to higher transport variability or additional dust input, for example, from

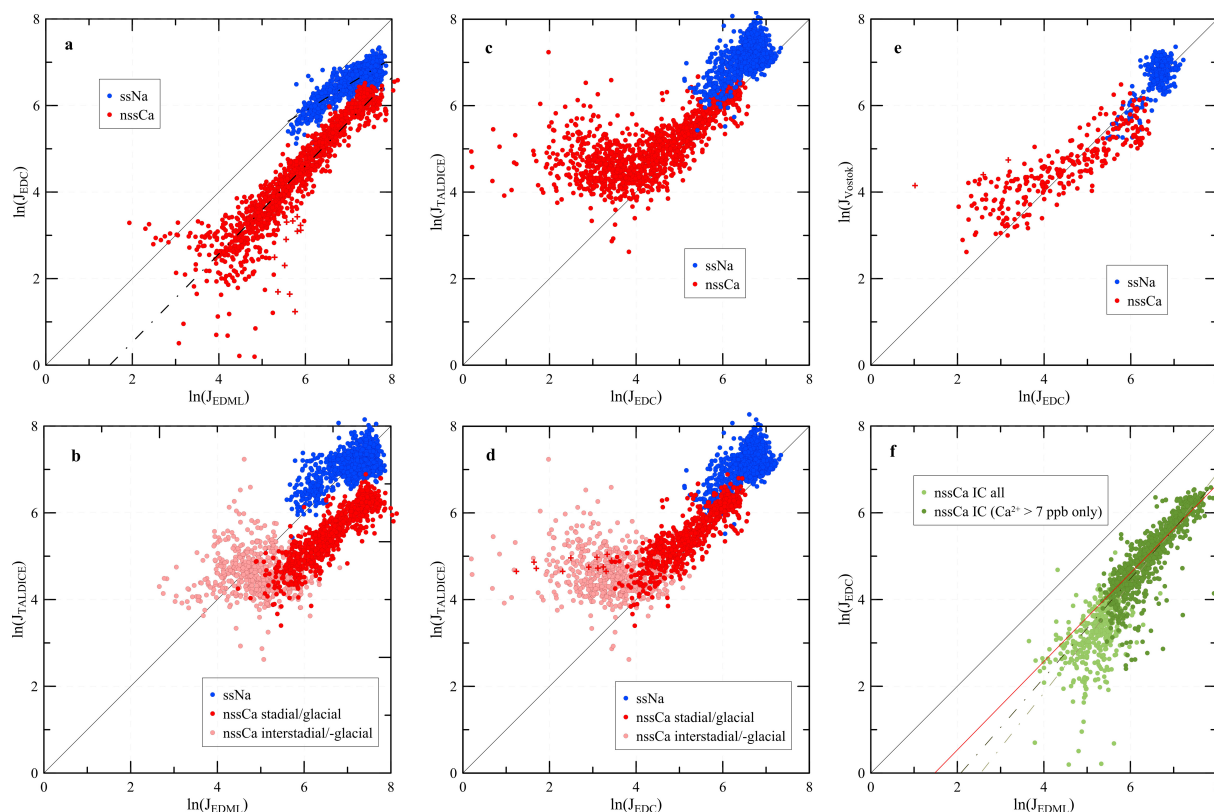


Fig. 6. Double-logarithmic scatter plots of the nssCa^{2+} (red) and ssNa^+ (blue) fluxes in 100 yr resolution (500 yr resolution for Vostok only). (a) EDC vs. EDML. The linear regression (dash-dotted line) shows a slope of 1 for nssCa^{2+} and of 0.6 for ssNa^+ . Outliers of the AIM 8 event are indicated as red crosses (see text for explanation). (b) TALDICE vs. EDML. Cold (dark red dots) and warm periods (light red dots) are discriminated in the nssCa^{2+} scatter plot. (c) TALDICE vs. EDC. The strong correlation of (a) is no longer persistent with these two ice cores when considering all climate periods of the past 150 ka. (d) TALDICE vs. EDC. The same data as in (c), however, cold (dark red dots) and warm periods (light red dots) are now discriminated. It becomes evident that during cold periods the linear correlation is still persistent, while for warm periods the two records are completely uncorrelated. EDC outliers during AIM 8 are indicated with red crosses. (e) Vostok vs. EDC. Vostok data were analysed using IC, thus, low nssCa^{2+} fluxes are biased towards higher values in the Vostok record. Data are shown in 500 yr resolution only. (f) EDML IC data versus EDC CFA data as shown in Fischer et al. (2007a). All data are shown in light green, in dark green only the data with original Ca^{2+} concentrations higher than 7 ppb. Linear regressions (dash-dotted lines) through all the IC data (light green, slope of the regression 1.26) and those above the 7 ppb threshold only (dark green, slope 1.13) show that the IC data set is indeed approaching the slope of the CFA data set as in (a) (red line, slope 1.02), when low concentration IC values are discarded.

Australia during warmer periods. This is also discussed from a climate model point-of-view in Sect. 3.5.

The atmospheric lifetime τ of dust particles has been modelled to be of the order of 3–10 days by previous studies with no significant changes over glacial/interglacial changes (e.g. Yung et al., 1996; Mahowald et al., 1999; Werner et al., 2002; Tegen, 2003). The transport time for aerosol from the Atlantic sector of the East Antarctic ice sheet (EDML) to the EDC and TALDICE drilling sites according to the results of our transport model is in the range of 1.2–1.5 times the atmospheric life time. This results in a transportation time of about 4–15 days in line with back trajectory studies (Reijmer et al., 2002; Scarchilli et al., 2011). In Table 2 we compiled $\Delta t/\tau$ between EDML and EDC for the major climate periods over the last 150 ka. Interestingly, $\Delta t/\tau$ gradually decreases

through time since the last interglacial period (see Table 2). However, it has to be acknowledged that these changes reported in Table 2 are small compared to the given standard deviation. Nevertheless, based on our ice core data we conclude that changes in transport and residence times of terrestrial aerosol are not subject to strong temporal changes and change only slowly on millennial timescales.

Fast source strength changes seem to be mainly responsible for the rapid changes in the dust input to the East Antarctic plateau. This is also in line with processes as described, for example, by Sugden et al. (2009), where potential dust mobilization is coupled to glacial melt-water deposition onto outwash plains in Patagonia. Other important parameters which govern continental aerosol source strength are surface wind speed, aridity, temperature, vegetation cover, soil

texture, and weathering (Bigler et al., 2010; Wolff et al., 2006). Most of those are fast reacting parameters compared to millennial timescale changes and thus corroborate the hypothesis of source strength changes being mainly responsible for rapid changes in dust input on the East Antarctic ice sheet.

3.4.2 Comparison of TALDICE versus EDML, EDC, and Vostok

In contrast to the EDC/EDML comparison, the good linear relationship between the logarithms of the nssCa^{2+} fluxes breaks down for TALDICE (Fig. 6c). Especially for lower concentrations, i.e. warmer conditions, there is a bias towards higher values in TALDICE. For this reason we divided the data in two groups, one for warm climate conditions the other for cold climate conditions. As a threshold between the two groups an arbitrary value of -38.9‰ in the $\delta^{18}\text{O}$ TALDICE record has been chosen (dashed line in the top panel of Fig. 3). In Fig. 6d the data shown in Fig. 6c are discriminated by this $\delta^{18}\text{O}$ threshold, resulting in two completely different regimes. While for cold climate conditions a linear relation between TALDICE and EDC exists ($r^2=0.75$, total number of data points $N=728$), the two nssCa^{2+} fluxes are completely uncorrelated ($r^2=0.02$, $N=588$) during warm periods. A similar behaviour can be observed when comparing TALDICE and EDML with strongly correlated nssCa^{2+} fluxes during cold periods ($r^2=0.77$, $N=759$) and no correlation during warm periods ($r^2=5 \times 10^{-6}$, $N=582$) (see Fig. 6b).

Furthermore, the calculated offset $\Delta t/\tau$ is close to zero for glacial conditions of TALDICE vs. EDC (Fig. 6d) indicating that the transport times to both drilling sites are almost equal (assuming the same τ for both transport paths as well as the same source region). The same observation is valid for the comparison of EDC with Vostok (see Fig. 6e) for the entire past 150 ka. However, it has to be considered that the Vostok data have been analysed with IC and show the same significant blank contribution for low Ca^{2+} concentrations as the IC data of EDML, resulting in a bias towards higher values in the Vostok data for low values (see Fig. 6e).

An offset $\Delta t/\tau$ close to zero for EDC vs. TALDICE as well as Vostok, respectively, is in agreement with studies based on back trajectories, which simulate the provenance of air parcels (Reijmer et al., 2002; Scarchilli et al., 2011) mostly originating from western pathways (dominated by the distinct Westerlies over the SO). However, recent simulations based on modern meteorological data suggest that a significant part of air masses to northern Victoria Land (i.e. Talos Dome) originate also from atypical pathways, i.e. southern and eastern pathways instead of the common western pathways (Scarchilli et al., 2011; Delmonte et al., 2013).

Higher nssCa^{2+} flux in TALDICE for warm climate conditions might also be explained by one or more additional local dust sources, which are only relevant for northern Victoria Land, but not for the East Antarctic plateau. Previous

studies on the isotopic signature ($^{87}\text{Sr}/^{86}\text{Sr}$ and $\epsilon_{\text{Nd}}(0)$) of interglacial dust from plateau ice cores show matching characteristics with dust from the Antarctic dry valleys (Delmonte et al., 2007). More recent studies of the isotopic signatures of dust particles in TALDICE, on the other hand, show good agreement also with dust samples taken from the Mesa Range, Nunataks at the margin of the Antarctic plateau and close to Talos Dome (Delmonte et al., 2010a, b, 2013). However, the identification of a local sub-region by isotopic signature analyses of potential source areas is complicated due to the ubiquitous mixing of the TALDICE dust samples with volcanic particles (Delmonte et al., 2013).

While the geographical proximity and altitude favours the contribution of the Mesa Range, the source strength of the Antarctic dry valleys is much enhanced during warm periods by glacial drift left behind from retreating glaciers, fluvial erosion and frost weathering due to temperatures above 0°C during the Antarctic summer. Furthermore, the ice-free areas in the Dry Valleys were substantially smaller or even completely covered by ice sheets during the last glacial period (Denton and Hughes, 2002; Huybrechts, 2002), which reduces the source strength drastically during these periods. As shown by Hall and Denton (2000) the Ross Sea was not only covered by an ice shelf during the LGM as it is today, but there was the Ross Sea Ice Sheet reaching down from the ground of the Ross Sea up into the Dry Valleys with an altitude of up to 350 m a.s.l. Johnson et al. (2008) have shown that the Cape Adare region (at the north eastern edge of northern Victoria land) was completely ice covered during the LGM and only became uncovered by ice at the transition into the Holocene at approx. 16 ka BP. In contrast, the Mesa Range was not covered by ice for the last 2 Myr as reconstructed by Oberholzer et al. (2008) by dating of moraines and erratic blocs with cosmogenic nuclides, involving a more constant source strength of the Mesa Range over glacial–interglacial and stadial–interstadial cycles. It is also possible that the dust source of the Mesa Range is partially depleted due to its long exposition to the atmosphere leading to a limited availability of mobile dust. Nonetheless, the flux of particles at Talos Dome associated to the local sources was similar during the LGM and the early Holocene (Albani et al., 2012a). Thus, we suggest that both proximal regions (Antarctic dry valleys and Mesa Range) are potential local source regions for dust input to Talos Dome and dedicated tracer studies are needed to provide the final answer.

3.5 Verification of our transport model by climate model data

In order to verify our transport model, we consider climate model simulations described in Albani et al. (2012b) and Mahowald et al. (2006). The model output fields allow one to plot the modelled dust deposition at EDML, EDC, Vostok, and TALDICE in the same way as done for the ice core data discussed above and shown in Figs. 6 and 7. Knowing

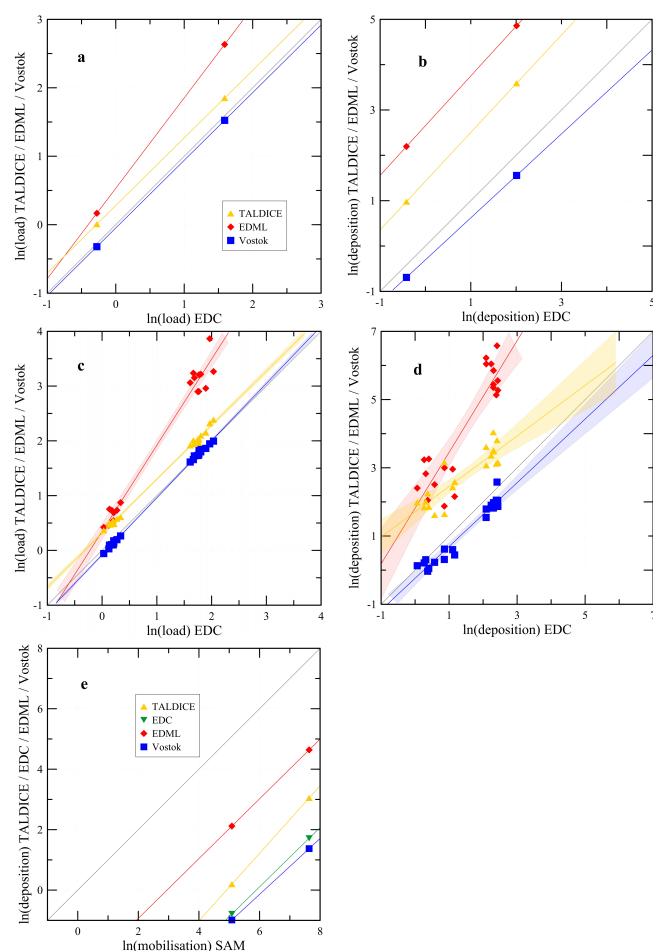


Fig. 7. (a) Dust column load of 1 yr tuned model runs at ice core grid points (Albani et al., 2012b). Double-logarithmic plots at EDML (red diamonds), Vostok (blue squares), and TALDICE (yellow triangles) vs. EDC. (b) Double-logarithmic plots of modelled dust deposition for all drill sites. The results are from the same model run as in (a). (c) Results of two 10 yr simulations showing inter-annual variability (10 points for each climate period) of the dust column load. Double-logarithmic scatter plots at EDML (red diamonds), Vostok (blue squares), and TALDICE (yellow triangles) vs. EDC, with the linear regressions including significance intervals (95 %) indicated in respective colours. See Table 2 for slopes, standard deviations, and r^2 values of the regressions shown in this figure. (d) Double-logarithmic plots of two 10 yr simulations for all drill sites showing inter-annual variability of the dust deposition. The results are from the same model run as in (c). Linear regressions including significance intervals (95 %) are indicated in respective colours. (e) Double logarithmic scatter plot of the source mobilisation vs. deposition showing the relation of dust deposited at the four ice core sites originating from a unique source (South America, SAM) based on the 1 yr tuned case of Albani et al. (2012b). Green triangles represent EDC.

the source emissions in the model allows us to explore the source–transport–deposition relations in a consistent framework. Our model allows for investigating equilibrium simulations from two climate periods, i.e. the current climate (representative of the Holocene) and the LGM.

For the exponential transport model, we considered the flux of ice core aerosol proxy data representative of the atmospheric aerosol concentration at the drill sites (see Sect. 2.3). For the model results, we consider modelled dust deposition flux and dust load at the drilling sites. A version of the model with the best accuracy in reproducing ice core deposition (and source apportionment) is the 1 yr tuned case from Albani et al. (2012b). Tuning was halving Australian emissions for current climate, and doubling it for the LGM, compared to a companion couple of runs spanning 10 years. The tuning yielded a better fit to the data for both climates. The results of the 1-year tuned model run show a slope close to one for the four ice cores (Fig. 7a) and give the source apportionment of Fig. 3 in Albani et al. (2012b).

A very similar behaviour can be observed when comparing the model results in Fig. 7a with the ice core data in Fig. 6. EDC, Vostok, and TALDICE model data show one-to-one relationships, with EDC and Vostok exhibiting a very small $\Delta t/\tau$ offset, thus exhibiting a nearly one-to-one relationship. Higher dust load for TALDICE and in particular for EDML (due to its proximity to the main source areas in southern South America) result in a distinct offset compared to EDC and Vostok, for both climate periods as also observed in the ice core data as well. In addition, the slope of the model results for EDML shows a slightly higher value.

If we now consider dust deposition instead of atmospheric surface concentration of the very same model run (Fig. 7b), we see all the regression lines having slopes close to one, but more distinct offsets. The uncertainty of the regression is unconstrained, as we are just using two points (average for current climate and LGM). Nevertheless, if we compare the 10 yr simulation using the same model but a different spatial pattern of emissions from the main source areas (Fig. 7d) with the 1 yr run of the very same simulation (not shown), we can infer that the slopes of the tuned 1 yr simulations are representative of the modelled relations, even though they are not the same for the tuned and the untuned version. Using the 10 yr results in slightly more scattered slopes for both dust load (Fig. 7c) and deposition flux (Fig. 7d), but allows for an estimation of the error and r^2 of the regression lines (in Table 3 the slopes, standard deviations, and r^2 values for all regressions shown in Fig. 7 are indicated).

Note that even for the 10 yr simulations, the linear regression in Fig. 7c and d is defined by two clouds of points representative for the climate and accumulation extremes during the Holocene and LGM. In contrast, the ice core data in Fig. 6 cover the whole spectrum of dust conditions from the glacial maximum to the Holocene, covering the long glaciations as well as the glacial–interglacial transition. This implies that the influence of the Holocene, characterised by the highest

Table 3. Slopes of the linear regressions calculated for the 10 yr model runs as shown in Fig. 7. The first line indicates the slopes of the dust deposition (dep.) (Fig. 7d), the second line those of the atmospheric dust load (Fig. 7c). The slopes of the regressions are indicated including the standard deviation, the respective r^2 values are indicated in parenthesis.

| | EDC vs. Vostok | EDC vs. EDML | EDC vs. TALDICE |
|------------|----------------------------|---------------------------|----------------------------|
| Deposition | 0.93 ± 0.06 (0.94) | 1.64 ± 0.19 (0.80) | 0.75 ± 0.10 (0.77) |
| Load | 1.04 ± 0.01 (0.999) | 1.57 ± 0.06 (0.98) | 0.99 ± 0.01 (0.997) |

precipitation rates, on the regression line is much smaller in the ice core data, as it represents only about a tenth of all data points used in the regression, while it represents 50 % of the data points defining the regression lines in Fig. 7. This effect may be partly responsible for the difference in the slope between data and model for EDML. Based on the overall good correspondence of the slopes of the regression lines for atmospheric dust loadings in Fig. 7a and c, we conclude that our transport model appears to be able to describe the transport effect on dust concentrations in different regions on the East Antarctic ice sheet.

The differences between the slopes in the modelled dust load and deposition (compare Fig. 7a/c with b/d) reflect the deposition processes in the model. For our exponential-decay transport model applied on the ice core flux data we only assume dry deposition (see Sect. 2.3), which is a reasonable approximation for interior sites such as EDC and Vostok (Wolff et al., 2006) and for all sites in the glacial, where snow accumulation was about 50 % lower than today, but may be inadequate in the case of peripheral sites such as EDML and Talos Dome for recent accumulation rate conditions. On the other hand, the Mahowald et al. (2006) model simulates both dry and wet deposition in proportions that are well represented for coastal Antarctic sites, but likely overestimate the contribution of wet deposition on the plateau (Albani et al., 2012b), thus leading to much larger differences in the logarithmic deposition fluxes in EDML and Talos Dome relative to EDC than in the modelled atmospheric concentrations.

A comparison of the ice core data $\Delta t/\tau$ offsets reported in Table 2 and shown in Fig. 6 with modelled ones (Fig. 7b and d) indicates that the modelled deposition is biased toward higher values for TALDICE and EDML, possibly in relation to overestimated precipitation rates in the model (Albani et al., 2012b). However, since the glacial/interglacial increase in snow deposition of a factor two is well captured by the model (Albani et al., 2012b), the one-to-one relationship is well reproduced, so there is a solid base to discuss the model results in comparison with the observations and making inferences on the underlying mechanisms, based on model physics.

With the model we can also explore the relation between source emissions from a specific area and the dust deposition. Considering emission and dust deposition from South America alone (Fig. 7e) gives a one-to-one relationship between logarithmic emission and deposition for all ice cores (only TALDICE has also a major Australian contribution in the model). This result is not surprising considering that the source experiencing the largest changes in modelled emissions is South America, with a factor 13 compared to a factor four for Australia (Albani et al., 2012b). In addition, the relative abundance of Patagonian dust for modelled dust deposition at ice core sites is either dominant (EDML) or increasing in the LGM for the other sites. Therefore, it is not surprising that southern South America is driving the slope, and may be the reason why the approximation of a unique source implicit in the exponential transport model holds in reproducing the one-to-one relationship, despite the observed complexity of the dust provenance mix especially in the Holocene (see Introduction).

The reason why the logarithms of TALDICE vs. EDC dust deposition in the model show a one-to-one relationship, which is not consistent with the ice core data due to the strong contribution of local sources at Talos Dome during the Holocene (see Sect. 3.4.2), is because the model does not consider local (Antarctic) sources. Thus, this particular feature in Talos Dome ice core data cannot be captured in the model.

The question remains whether constant transport efficiency (i.e. constant $\Delta t/\tau$) represents a unique solution to explain the regression lines in Fig. 6, or whether changes in the source mix may also allow for a one-to-one relationship between different ice core sites in Antarctica. Interestingly, the Mahowald et al. (2006) model simulates a decrease in dust lifetime (τ) in the glacial from 3.2 to 2.7 days for the southern high latitudes $> 60^\circ$ S (Albani et al., 2012b). This would increase the slope in Fig. 7, if transport times were constant. At the same time a metric for transport efficiency in the model (the ratio of dust load/deposition to the emissions) is increased both for Australia and South America in the glacial. This implies a more focused/direct transport from South America, possibly indicating shorter transport times. Overall the deposition efficiency, which summarises the mentioned changes in transport and lifetimes, tends to increase for the sites of interest, but at different rates and with spatial patterns depending on the source (Figs. 8 and 9 in Albani et al., 2012b). In conclusion the model described in Albani et al. (2012b) would support only partly balancing effects in dust lifetimes and transport time on dust exported from southern South America. This would tend to support the idea that the one-to-one relation is also consistent with a more complex scenario involving changes in the source mix and parallel changes in transport and residence time of dust. Uncertainties still exist in modelled dust fluxes, as the model is still not able to quantitatively reproduce the glacial–interglacial deposition fluxes for all the ice

cores in Antarctica (Albani et al., 2012b). Future improved model studies will help to better disentangle the source and transport contributions to glacial–interglacial dust changes in Antarctica.

4 Conclusions

In this study we presented new CFA nssCa^{2+} and ssNa^+ records of the Talos Dome ice core in centennial resolution reaching back 150 ka BP. TALDICE nssCa^{2+} flux shows both large-scale changes on glacial/interglacial timescales as well as a regional signal, emerging when dust advection from remote sources was extremely low, that is, during warm (interglacial) periods. Dust deposition at Talos Dome generally reflects major climate changes on a hemispheric scale during the last 150 ka. However, the significant contribution of proximal dust sources during warm climate periods (e.g. the Holocene) makes Talos Dome sensitive to regional atmospheric circulation changes.

Our new nssCa^{2+} and ssNa^+ flux records corroborate the scenario proposed by Albani et al. (2012a), suggesting that more frequent air mass trajectories through the Ross Sea are mainly responsible for a reduced dust input from local sources after 8 ka BP. Since there are no TALDICE nssCa^{2+} and ssNa^+ data available for the late Holocene, we cannot examine the behaviour of the two parameters in the context of a late Holocene Ross ice shelf re-advance (Albani et al., 2012a). An extension of the existing records to the last three millennia would allow for a verification of an according behaviour. Nevertheless, based on the new TALDICE mineral dust and sea ice proxy records we suggest similar regional climate conditions as observed during the Holocene prevailing also during the last interglacial period in the Ross Sea area. In particular, our new ssNa^+ data indicate the presence of extended sea ice cover in the Ross Sea area during MIS 5.5 of similar extent as during the Holocene.

Two potential local source regions, the Antarctic dry valleys and/or the Mesa Range, which could not be discriminated unambiguously as main contributors to local dust input to Talos Dome so far, may contribute to the higher dust fluxes during warm periods compared to the other ice core sites. The Dry Valleys are considered to be an efficient dust source because glacial drift deposits, fluvial erosion, and frost weathering enhance the availability of mobile dust during warm periods, while during cold periods this source region is ice covered and thus no longer active in line with our new TALDICE nssCa^{2+} data. On the other hand, sources in the Mesa Range lie at high elevation and much closer to the site. They are smaller compared to the Dry Valleys and possibly in part depleted because of the long exposure, but at the same time they were ice free throughout the glacial period, consistent with the dust coarse particle flux (Albani et al., 2012a).

The availability of three highly resolved nssCa^{2+} records (EDC, EDML, and TALDICE, respectively) allow for a revision of the estimate on atmospheric CO_2 sensitivity to dust induced iron fertilisation in the SO. Röthlisberger et al. (2004) based their estimation on the only record available at that time (CFA nssCa^{2+} of EDC) including extremely low values during AIM 8 which, however, have not been observed in other ice core records. Accordingly, their finding of 20 ppm seems to underestimate the CO_2 sensitivity. In a revised estimation, including nssCa^{2+} of TALDICE, EDML, and EDC, and discarding the extreme low EDC values during AIM 8, we estimate the increase of atmospheric CO_2 during T1 linked to reduced dust induced iron fertilisation in the SO to be up to 40 ppm.

Based on our exponential transport model applied on nssCa^{2+} records of four East Antarctic ice cores we cannot see any long range transport effects influencing atmospheric dust concentration changes in East Antarctica. A comparison with climate model results confirm our findings of constant transport efficiencies (i.e. $\Delta t/\tau$) for dust fluxes at the four drill sites for Holocene/LGM climate. The model, however, allows that the one-to-one relationship of dust fluxes at the four drill sites would be also consistent with a more complex scenario where transport changes are compensated by a changing source mix. Nevertheless, we can conclude that the observed nssCa^{2+} flux changes predominantly reflect changes in southern South America source strength during the past 150 ka. Changing transport time and atmospheric residence time may have contributed to determining the magnitude of the observed flux changes.

Supplementary material related to this article is available online at <http://www.clim-past.net/9/2789/2013/cp-9-2789-2013-supplement.zip>.

Acknowledgements. We thank the AWI team, in particular Anna Wegner and Birthe Twarloh, as well as Matthias Bigler and Christof Bernhard for their support during the CFA analyses. This research is funded by the Swiss National Science Foundation and the Prince Albert II of Monaco foundation. The Talos Dome Ice core Project (TALDICE), a joint European programme, is funded by national contributions from Italy, France, Germany, Switzerland and the UK. Primary logistical support was provided by PNRA at Talos Dome. This is TALDICE publication no. 35.

Edited by: E. Isaksson

References

Abram, N. J., Wolff, E. W., and Curran, M. A. J.: A review of sea ice proxy information from polar ice cores, *Quaternary Sci. Rev.*, 79, 168–183, doi:10.1016/j.quascirev.2013.01.011, 2013.

- Albani, S., Delmonte, B., Maggi, V., Baroni, C., Petit, J.-R., Stenni, B., Mazzola, C., and Frezzotti, M.: Interpreting last glacial to Holocene dust changes at Talos Dome (East Antarctica): implications for atmospheric variations from regional to hemispheric scales, *Clim. Past*, 8, 741–750, doi:10.5194/cp-8-741-2012, 2012a.
- Albani, S., Mahowald, N., Delmonte, B., Maggi, V., and Winckler, G.: Comparing modeled and observed changes in mineral dust transport and deposition to Antarctica between the Last Glacial Maximum and current climates, *Clim. Dynam.*, 38, 1731–1755, doi:10.1007/s00382-011-1139-5, 2012b.
- Archer, D., Winguth, A., Lea, D., and Mahowald, N.: What caused the glacial/interglacial atmospheric $p\text{CO}_2$ cycles?, *Rev. Geophys.*, 38, 159–189, doi:10.1029/1999rg000066, 2000.
- Basile, I., Grousset, F. E., Revel, M., Petit, J. R., Biscaye, P. E., and Barkov, N. I.: Patagonian origin of glacial dust deposited in East Antarctica (Vostok and Dome C) during glacial stages 2, 4 and 6, *Earth Planet. Sc. Lett.*, 146, 573–589, doi:10.1016/S0012-821X(96)00255-5, 1997.
- Bazin, L., Landais, A., Lemieux-Dudon, B., Toyé Mahamadou Kele, H., Veres, D., Parrenin, F., Martinerie, P., Ritz, C., Capron, E., Lipenkov, V., Loutre, M.-F., Raynaud, D., Vinther, B., Svensson, A., Rasmussen, S. O., Severi, M., Blunier, T., Leuenberger, M., Fischer, H., Masson-Delmotte, V., Chappellaz, J., and Wolff, E.: An optimized multi-proxy, multi-site Antarctic ice and gas orbital chronology (AICC2012): 120–800 ka, *Clim. Past*, 9, 1715–1731, doi:10.5194/cp-9-1715-2013, 2013.
- Bereiter, B., Lüthi, D., Siegrist, M., Schüpbach, S., Stocker, T. F., and Fischer, H.: Mode change of millennial CO_2 variability during the last glacial cycle associated with a bipolar marine carbon seesaw, *P. Natl. Acad. Sci.*, 109, 9755–9760, doi:10.1073/pnas.1204069109, 2012.
- Bigler, M., Röthlisberger, R., Lambert, F., Stocker, T. F., and Wagenbach, D.: Aerosol deposited in East Antarctica over the last glacial cycle: Detailed apportionment of continental and sea-salt contributions, *J. Geophys. Res.*, 111, D08205, doi:10.1029/2005JD006469, 2006.
- Bigler, M., Röthlisberger, R., Lambert, F., Wolff, E. W., Castellano, E., Udristi, R., Stocker, T. F., and Fischer, H.: Atmospheric decadal variability from high-resolution Dome C ice core records of aerosol constituents beyond the Last Interglacial, *Quaternary Sci. Rev.*, 29, 324–337, doi:10.1016/j.quascirev.2009.09.009, 2010.
- Blunier, T., Schwander, J., Stauffer, B., Stocker, T., Dällenbach, A., Indermühle, A., Tschumi, J., Chappellaz, J., Raynaud, D., and Barnola, J. M.: Timing of the Antarctic Cold Reversal and the atmospheric CO_2 increase with respect to the Younger Dryas event, *Geophys. Res. Lett.*, 24, 2683–2686, doi:10.1029/97GL02658, 1997.
- Bory, A., Wolff, E., Mulvaney, R., Jagoutz, E., Wegner, A., Ruth, U., and Elderfield, H.: Multiple sources supply eolian mineral dust to the Atlantic sector of coastal Antarctica: Evidence from recent snow layers at the top of Berkner Island ice sheet, *Earth Planet. Sc. Lett.*, 291, 138–148, doi:10.1016/j.epsl.2010.01.006, 2010.
- Bouttes, N., Paillard, D., and Roche, D. M.: Impact of brine-induced stratification on the glacial carbon cycle, *Clim. Past*, 6, 575–589, doi:10.5194/cp-6-575-2010, 2010.
- Brook, E. J., White, J. W. C., Schilla, A. S. M., Bender, M. L., Barnett, B., Severinghaus, J. P., Taylor, K. C., Alley, R. B., and Steig, E. J.: Timing of millennial-scale climate change at Siple Dome, West Antarctica, during the last glacial period, *Quaternary Sci. Rev.*, 24, 1333–1343, doi:10.1016/j.quascirev.2005.02.002, 2005.
- Buiron, D., Chappellaz, J., Stenni, B., Frezzotti, M., Baumgartner, M., Capron, E., Landais, A., Lemieux-Dudon, B., Masson-Delmotte, V., Montagnat, M., Parrenin, F., and Schilt, A.: TALDICE-1 age scale of the Talos Dome deep ice core, East Antarctica, *Clim. Past*, 7, 1–16, doi:10.5194/cp-7-1-2011, 2011.
- De Angelis, M., Steffensen, J. P., Legrand, M., Clausen, H., and Hammer, C.: Primary aerosol (sea salt and soil dust) deposited in Greenland ice during the last climatic cycle: Comparison with east Antarctic records, *J. Geophys. Res.-Oceans*, 102, 26681–26698, doi:10.1029/97jc01298, 1997.
- Delmonte, B., Petit, J. R., Basile-Doelsch, I., Jagoutz, E., and Maggi, V.: Developments in Quaternary Sciences, vol. 7, chap. 6: Late quaternary interglacials in East Antarctica from ice-core dust records, Elsevier, 53–73, 2007.
- Delmonte, B., Andersson, P. S., Hansson, M., Schöberg, H., Petit, J. R., Basile-Doelsch, I., and Maggi, V.: Aeolian dust in East Antarctica (EPICA-Dome C and Vostok): Provenance during glacial ages over the last 800 kyr, *Geophys. Res. Lett.*, 35, L07703, doi:10.1029/2008GL033382, 2008.
- Delmonte, B., Andersson, P. S., Schöberg, H., Hansson, M., Petit, J. R., Delmas, R., Gaiero, D. M., Maggi, V., and Frezzotti, M.: Geographic provenance of aeolian dust in East Antarctica during Pleistocene glaciations: preliminary results from Talos Dome and comparison with East Antarctic and new Andean ice core data, *Quaternary Sci. Rev.*, 29, 256–264, doi:10.1016/j.quascirev.2009.05.010, 2010a.
- Delmonte, B., Baroni, C., Andersson, P. S., Schöberg, H., Hansson, M., Aciego, S., Petit, J. R., Albani, S., Mazzola, C., Maggi, V., and Frezzotti, M.: Aeolian dust in the Talos Dome ice core (East Antarctica, Pacific/Ross Sea sector): Victoria Land versus remote sources over the last two climate cycles, *J. Quaternary Sci.*, 25, 1327–1337, doi:10.1002/jqs.1418, 2010b.
- Delmonte, B., Baroni, C., Andersson, P. S., Narcisi, B., Salvatore, M. C., Petit, J. R., Scarchilli, C., Frezzotti, M., Albani, S., and Maggi, V.: Modern and Holocene aeolian dust variability from Talos Dome (Northern Victoria Land) to the interior of the Antarctic ice sheet, *Quaternary Sci. Rev.*, 64, 76–89, doi:10.1016/j.quascirev.2012.11.033, 2013.
- Denton, G. H. and Hughes, T. J.: Reconstructing the Antarctic Ice Sheet at the Last Glacial Maximum, *Quaternary Sci. Rev.*, 21, 193–202, doi:10.1016/S0277-3791(01)00090-7, 2002.
- Dieckmann, G. S. and Hellmer, H. H.: The Importance of Sea Ice: An Overview, Wiley-Blackwell, 1–22, 2010.
- EPICA, C. M.: Eight glacial cycles from an Antarctic ice core, *Nature*, 429, 623–628, doi:10.1038/nature02599, 2004.
- EPICA, C. M.: One-to-one coupling of glacial climate variability in Greenland and Antarctica, *Nature*, 444, 195–198, doi:10.1038/nature05301, 2006.
- Fischer, H., Fundel, F., Ruth, U., Twarloh, B., Wegner, A., Udristi, R., Becagli, S., Castellano, E., Morganti, A., Severi, M., Wolff, E. W., Littot, G., Röthlisberger, R., Mulvaney, R., Hutterli, M. A., Kaufmann, P., Federer, U., Lambert, F., Bigler, M., Hansson, M., Jonsell, U., de Angelis, M., Boutron, C., Siggaard-Andersen,

- M.-L., Steffensen, J. P., Barbante, C., Gaspari, V., Gabrielli, P., and Wagenbach, D.: Reconstruction of millennial changes in dust emission, transport and regional sea ice coverage using the deep EPICA ice cores from the Atlantic and Indian Ocean sector of Antarctica, *Earth Planet. Sc. Lett.*, 260, 340–354, doi:10.1016/j.epsl.2007.06.014, 2007a.
- Fischer, H., Siggaard-Andersen, M.-L., Ruth, U., Röthlisberger, R., and Wolff, E. W.: Glacial/interglacial changes in mineral dust and sea-salt records in polar ice cores: Sources, transport, and deposition, *Rev. Geophys.*, 45, RG1002, doi:10.1029/2005RG000192, 2007b.
- Fischer, H., Schmitt, J., Lüthi, D., Stocker, T. F., Tschumi, T., Parekh, P., Joos, F., Köhler, P., Völker, C., Gersonde, R., Barbante, C., Le Floch, M., Raynaud, D., and Wolff, E.: The role of Southern Ocean processes in orbital and millennial CO₂ variations – A synthesis, *Quaternary Sci. Rev.*, 29, 193–205, doi:10.1016/j.quascirev.2009.06.007, 2010.
- Frezzotti, M., Urbini, S., Proposito, M., Scarchilli, C., and Gandolfi, S.: Spatial and temporal variability of surface mass balance near Talos Dome, East Antarctica, *J. Geophys. Res.*, 112, F02032, doi:10.1029/2006jf000638, 2007.
- Gabrielli, P., Wegner, A., Petit, J. R., Delmonte, B., De Deckker, P., Gaspari, V., Fischer, H., Ruth, U., Kriews, M., Boutron, C., Cescon, P., and Barbante, C.: A major glacial-interglacial change in aeolian dust composition inferred from Rare Earth Elements in Antarctic ice, *Quaternary Sci. Rev.*, 29, 265–273, doi:10.1016/j.quascirev.2009.09.002, 2010.
- Gaiero, D. M.: Dust provenance in Antarctic ice during glacial periods: From where in southern South America?, *Geophys. Res. Lett.*, 34, L17707, doi:10.1029/2007gl030520, 2007.
- Gaspari, V., Barbante, C., Cozzi, G., Cescon, P., Boutron, C. F., Gabrielli, P., Capodaglio, G., Ferrari, C., Petit, J. R., and Delmonte, B.: Atmospheric iron fluxes over the last deglaciation: Climatic implications, *Geophys. Res. Lett.*, 33, L03704, doi:10.1029/2005gl024352, 2006.
- Gersonde, R., Crosta, X., Abelmann, A., and Armand, L.: Sea-surface temperature and sea ice distribution of the Southern Ocean at the EPILOG Last Glacial Maximum—a circum-Antarctic view based on siliceous microfossil records, *Quaternary Sci. Rev.*, 24, 869–896, doi:10.1016/j.quascirev.2004.07.015, 2005.
- Hall, B. L. and Denton, G. H.: Extent and Chronology of the Ross Sea Ice Sheet and the Wilson Piedmont Glacier along the Scott Coast at and since the Last Glacial Maximum, *Geogr. Ann. A*, 82, 337–363, doi:10.1111/j.0435-3676.2000.00128.x, 2000.
- Huybrechts, P.: Sea-level changes at the LGM from ice-dynamic reconstructions of the Greenland and Antarctic ice sheets during the glacial cycles, *Quaternary Sci. Rev.*, 21, 203–231, doi:10.1016/S0277-3791(01)00082-8, 2002.
- Johnson, J. S., Hillenbrand, C.-D., Smellie, J. L., and Rocchi, S.: The last deglaciation of Cape Adare, northern Victoria Land, Antarctica, *Antarct. Sci.*, 20, 581–587, doi:10.1017/S0954102008001417, 2008.
- Jouzel, J., Masson-Delmotte, V., Cattani, O., Dreyfus, G., Falourd, S., Hoffmann, G., Minster, B., Nouet, J., Barnola, J. M., Chappellaz, J., Fischer, H., Gallet, J. C., Johnsen, S., Leuenberger, M., Loulergue, L., Lüthi, D., Oerter, H., Parrenin, F., Raisbeck, G., Raynaud, D., Schilt, A., Schwander, J., Selmo, E., Souchez, R., Spahni, R., Stauffer, B., Steffensen, J. P., Stenni, B., Stocker, T. F., Tison, J. L., Werner, M., and Wolff, E. W.: Orbital and Millennial Antarctic Climate Variability over the Past 800,000 Years, *Science*, 317, 793–796, doi:10.1126/science.1141038, 2007.
- Kaufmann, P. R., Federer, U., Hutterli, M. A., Bigler, M., Schüpbach, S., Ruth, U., Schmitt, J., and Stocker, T. F.: An Improved Continuous Flow Analysis System for High-Resolution Field Measurements on Ice Cores, *Environ. Sci. Technol.*, 42, 8044–8050, doi:10.1021/es8007722, 2008.
- Kaufmann, P. R., Fundel, F., Fischer, H., Bigler, M., Ruth, U., Udisti, R., Hansson, M., de Angelis, M., Barbante, C., Wolff, E. W., Hutterli, M. A., and Wagenbach, D.: Ammonium and non-sea salt sulfate in the EPICA ice cores as indicator of biological activity in the Southern Ocean, *Quaternary Sci. Rev.*, 29, 313–323, doi:10.1016/j.quascirev.2009.11.009, 2010.
- Knorr, G. and Lohmann, G.: Southern Ocean origin for the resumption of Atlantic thermohaline circulation during deglaciation, *Nature*, 424, 532–536, doi:10.1038/nature01855, 2003.
- Krinner, G. and Genthon, C.: GCM simulations of the Last Glacial Maximum surface climate of Greenland and Antarctica, *Clim. Dynam.*, 14, 741–758, doi:10.1007/s003820050252, 1998.
- Krinner, G. and Genthon, C.: Tropospheric transport of continental tracers towards Antarctica under varying climatic conditions, *Tellus B*, 55, 54–70, doi:10.1034/j.1600-0889.2003.00004.x, 2003.
- Lambert, F., Delmonte, B., Petit, J. R., Bigler, M., Kaufmann, P. R., Hutterli, M. A., Stocker, T. F., Ruth, U., Steffensen, J. P., and Maggi, V.: Dust-climate couplings over the past 800,000 years from the EPICA Dome C ice core, *Nature*, 452, 616–619, doi:10.1038/nature06763, 2008.
- Lemieux-Dudon, B., Blayo, E., Petit, J.-R., Waelbroeck, C., Svensson, A., Ritz, C., Barnola, J.-M., Narcisi, B. M., and Parrenin, F.: Consistent dating for Antarctic and Greenland ice cores, *Quaternary Sci. Rev.*, 29, 8–20, doi:10.1016/j.quascirev.2009.11.010, 2010.
- Li, F., Ginoux, P., and Ramaswamy, V.: Distribution, transport, and deposition of mineral dust in the Southern Ocean and Antarctica: Contribution of major sources, *J. Geophys. Res. Atmos.*, 113, D10207, doi:10.1029/2007jd009190, 2008.
- Mahowald, N. M., Kohfeld, K., Hansson, M., Balkanski, Y., Harrison, S. P., Prentice, I. C., Schulz, M., and Rodhe, H.: Dust sources and deposition during the last glacial maximum and current climate: A comparison of model results with paleodata from ice cores and marine sediments, *J. Geophys. Res.-Atmos.*, 104, 15895–15916, doi:10.1029/1999jd900084, 1999.
- Mahowald, N. M., Muhs, D. R., Levis, S., Rasch, P. J., Yoshioka, M., Zender, C. S., and Luo, C.: Change in atmospheric mineral aerosols in response to climate: Last glacial period, preindustrial, modern, and doubled carbon dioxide climates, *J. Geophys. Res.-Atmos.*, 111, D10202, doi:10.1029/2005jd006653, 2006.
- Marino, F., Castellano, E., Nava, S., Chiari, M., Ruth, U., Wegner, A., Lucarelli, F., Udisti, R., Delmonte, B., and Maggi, V.: Coherent composition of glacial dust on opposite sides of the East Antarctic Plateau inferred from the deep EPICA ice cores, *Geophys. Res. Lett.*, 36, L23703, doi:10.1029/2009gl040732, 2009.
- Martin, J. H.: Glacial-interglacial CO₂ change: The Iron Hypothesis, *Paleoceanography*, 5, 1–13, doi:10.1029/PA005i001p00001, 1990.
- Martínez-García, A., Rosell-Melé, A., Jaccard, S. L., Geibert, W., Sigman, D. M., Haug, G. H.: Southern Ocean dust-climate

- coupling over the past four million years, *Nature*, 476, 312–315, doi:10.1038/nature10310, 2011.
- McKay, R., Naish, T., Powell, R., Barrett, P., Scherer, R., Talarico, F., Kyle, P., Monien, D., Kuhn, G., Jackolski, C., and Williams, T.: Pleistocene variability of Antarctic Ice Sheet extent in the Ross Embayment, *Quaternary Sci. Rev.*, 34, 93–112, doi:10.1016/j.quascirev.2011.12.012, 2012.
- Oberholzer, P., Baroni, C., Salvatore, M., Baur, H., and Wieler, R.: Dating late Cenozoic erosional surfaces in Victoria Land, Antarctica, with cosmogenic neon in pyroxenes, *Antarct. Sci.*, 20, 89–98, doi:10.1017/S095410200700079X, 2008.
- Petit, J. R. and Delmonte, B.: A model for large glacial-interglacial climate-induced changes in dust and sea salt concentrations in deep ice cores (central Antarctica): palaeoclimatic implications and prospects for refining ice core chronologies, *Tellus B*, 61, 768–790, doi:10.1111/j.1600-0889.2009.00437.x, 2009.
- Petit, J. R., Mournier, L., Jouzel, J., Korotkevich, Y. S., Kotlyakov, V. I., and Lorius, C.: Palaeoclimatological and chronological implications of the Vostok core dust record, *Nature*, 343, 56–58, doi:10.1038/343056a0, 1990.
- Petit, J. R., Jouzel, J., Raynaud, D., Barkov, N. I., Barnola, J. M., Basile, I., Bender, M., Chappellaz, J., Davis, M., Delaygue, G., Delmotte, M., Kotlyakov, V. M., Legrand, M., Lipenkov, V. Y., Lorius, C., Pepin, L., Ritz, C., Saltzman, E., and Stievenard, M.: Climate and atmospheric history of the past 420,000 years from the Vostok ice core, Antarctica, *Nature*, 399, 429–436, doi:10.1038/20859, 1999.
- Rankin, A. M., Auld, V., and Wolff, E. W.: Frost flowers as a source of fractionated sea salt aerosol in the polar regions, *Geophys. Res. Lett.*, 27, 3469–3472, doi:10.1029/2000gl011771, 2000.
- Reijmer, C. H., van den Broeke, M. R., and Scheele, M. P.: Air Parcel Trajectories and Snowfall Related to Five Deep Drilling Locations in Antarctica Based on the ERA-15 Dataset, *J. Climate*, 15, 1957–1968, doi:10.1175/1520-0442(2002)015<1957:APTASR>2.0.CO;2, 2002.
- Revel-Rolland, M., De Deckker, P., Delmonte, B., Hesse, P. P., Magee, J. W., Basile-Doelsch, I., Grousset, F., and Bosch, D.: Eastern Australia: A possible source of dust in East Antarctica interglacial ice, *Earth Planet. Sc. Lett.*, 249, 1–13, doi:10.1016/j.epsl.2006.06.028, 2006.
- Röthlisberger, R., Bigler, M., Hutterli, M. A., Sommer, S., Stauffer, B., Junghans, H. G., and Wagenbach, D.: Technique for Continuous High-Resolution Analysis of Trace Substances in Firn and Ice Cores, *Environ. Sci. Technol.*, 34, 338–342, doi:10.1021/es9907055, 2000.
- Röthlisberger, R., Mulvaney, R., Wolff, E. W., Hutterli, M. A., Bigler, M., Sommer, S., and Jouzel, J.: Dust and sea salt variability in central East Antarctica (Dome C) over the last 45 kyrs and its implications for southern high-latitude climate, *Geophys. Res. Lett.*, 29, 1963, doi:10.1029/2002GL015186, 2002.
- Röthlisberger, R., Bigler, M., Wolff, E. W., Joos, F., Monnin, E., and Hutterli, M. A.: Ice core evidence for the extent of past atmospheric CO₂ change due to iron fertilisation, *Geophys. Res. Lett.*, 31, L16207, doi:10.1029/2004GL020338, 2004.
- Röthlisberger, R., Crosta, X., Abram, N. J., Armand, L., and Wolff, E. W.: Potential and limitations of marine and ice core sea ice proxies: an example from the Indian Ocean sector, *Quaternary Sci. Rev.*, 29, 296–302, doi:10.1016/j.quascirev.2009.10.005, 2010.
- Scarchilli, C., Frezzotti, M., and Ruti, P.: Snow precipitation at four ice core sites in East Antarctica: provenance, seasonality and blocking factors, *Clim. Dynam.*, 37, 2107–2125, doi:10.1007/s00382-010-0946-4, 2011.
- Sime, L. C., Kohfeld, K. E., Le Quééré, C., Wolff, E. W., de Boer, A. M., Graham, R. M., and Bopp, L.: Southern Hemisphere westerly wind changes during the Last Glacial Maximum: model-data comparison, *Quaternary Sci. Rev.*, 64, 104–120, doi:10.1016/j.quascirev.2012.12.008, 2013.
- Spolaor, A., Vallelonga, P., Cozzi, G., Gabrieli, J., Varin, C., Kehrwald, N., Zennaro, P., Boutron, C., and Barbante, C.: Iron speciation in aerosol dust influences iron bioavailability over glacial-interglacial timescales, *Geophys. Res. Lett.*, 40, 1618–1623, doi:10.1002/grl.50296, 2013.
- Stenni, B., Buiron, D., Frezzotti, M., Albani, S., Barbante, C., Bard, E., Barnola, J. M., Baroni, M., Baumgartner, M., Bonazza, M., Capron, E., Castellano, E., Chappellaz, J., Delmonte, B., Falourd, S., Genoni, L., Iacumin, P., Jouzel, J., Kipfstuhl, S., Landais, A., Lemieux-Dudon, B., Maggi, V., Masson-Delmotte, V., Mazzola, C., Minster, B., Montagnat, M., Mulvaney, R., Narcisi, B., Oerter, H., Parrenin, F., Petit, J. R., Ritz, C., Scarchilli, C., Schilt, A., Schüpbach, S., Schwander, J., Selmo, E., Severi, M., Stocker, T. F., and Udisti, R.: Expression of the bipolar see-saw in Antarctic climate records during the last deglaciation, *Nat. Geosci.*, 4, 46–49, doi:10.1038/ngeo1026, 2011.
- Stocker, T. F. and Johnsen, S. J.: A minimum thermodynamic model for the bipolar seesaw, *Paleoceanography*, 18, 1087, doi:10.1029/2003PA000920, 2003.
- Sugden, D. E., McCulloch, R. D., Bory, A. J. M., and Hein, A. S.: Influence of Patagonian glaciers on Antarctic dust deposition during the last glacial period, *Nat. Geosci.*, 2, 281–285, doi:10.1038/ngeo474, 2009.
- Tegen, I.: Modeling the mineral dust aerosol cycle in the climate system, *Quaternary Sci. Rev.*, 22, 1821–1834, doi:10.1016/S0277-3791(03)00163-X, 2003.
- Toggweiler, J. R.: Variation of atmospheric CO₂ by ventilation of the ocean's deepest water, *Paleoceanography*, 14, 571–588, doi:10.1029/1999pa900033, 1999.
- Toggweiler, J. R., Russell, J. L., and Carson, S. R.: Mid-latitude westerlies, atmospheric CO₂, and climate change during the ice ages, *Paleoceanography*, 21, PA2005, doi:10.1029/2005pa001154, 2006.
- Vallelonga, P., Barbante, C., Cozzi, G., Gabrieli, J., Schüpbach, S., Spolaor, A., and Turetta, C.: Iron fluxes to Talos Dome, Antarctica, over the past 200 kyr, *Clim. Past*, 9, 597–604, doi:10.5194/cp-9-597-2013, 2013.
- Veres, D., Bazin, L., Landais, A., Toyé Mahamadou Kele, H., Lemieux-Dudon, B., Parrenin, F., Martinerie, P., Blayo, E., Blunier, T., Capron, E., Chappellaz, J., Rasmussen, S. O., Severi, M., Svensson, A., Vinther, B., and Wolff, E. W.: The Antarctic ice core chronology (AICC2012): an optimized multi-parameter and multi-site dating approach for the last 120 thousand years, *Clim. Past*, 9, 1733–1748, doi:10.5194/cp-9-1733-2013, 2013.
- Wagenbach, D., Ducroz, F., Mulvaney, R., Keck, L., Minikin, A., Legrand, M., Hall, J. S., and Wolff, E. W.: Sea-salt aerosol in coastal Antarctic regions, *J. Geophys. Res.*, 103, 10961–10974, doi:10.1029/97JD01804, 1998.
- Weber, M. E., Kuhn, G., Spreng, D., Rolf, C., Ohlwein, C., and Ricken, W.: Dust transport from Patagonia to Antarctica → A

- new stratigraphic approach from the Scotia Sea and its implications for the last glacial cycle, *Quaternary Sci. Rev.*, 36, 177–188, doi:10.1016/j.quascirev.2012.01.016, 2012.
- Wegner, A., Gabrielli, P., Wilhelms-Dick, D., Ruth, U., Kriews, M., De Deckker, P., Barbante, C., Cozzi, G., Delmonte, B., and Fischer, H.: Change in dust variability in the Atlantic sector of Antarctica at the end of the last deglaciation, *Clim. Past*, 8, 135–147, doi:10.5194/cp-8-135-2012, 2012.
- Werner, M., Tegen, I., Harrison, S. P., Kohfeld, K. E., Prentice, I. C., Balkanski, Y., Rodhe, H., and Roelandt, C.: Seasonal and inter-annual variability of the mineral dust cycle under present and glacial climate conditions, *J. Geophys. Res.-Atmos.*, 107, 4744, doi:10.1029/2002jd002365, 2002.
- Wolff, E. W., Rankin, A. M., and Röthlisberger, R.: An ice core indicator of Antarctic sea ice production?, *Geophys. Res. Lett.*, 30, 2158, doi:10.1029/2003GL018454, 2003.
- Wolff, E. W., Fischer, H., Fundel, F., Ruth, U., Twarloh, B., Littot, G. C., Mulvaney, R., Röthlisberger, R., de Angelis, M., Boutron, C. F., Hansson, M., Jonsell, U., Hutterli, M. A., Lambert, F., Kaufmann, P., Stauffer, B., Stocker, T. F., Steffensen, J. P., Bigler, M., Siggaard-Andersen, M. L., Udasti, R., Becagli, S., Castellano, E., Severi, M., Wagenbach, D., Barbante, C., Gabrielli, P., and Gaspari, V.: Southern Ocean sea-ice extent, productivity and iron flux over the past eight glacial cycles, *Nature*, 440, 491–496, doi:10.1038/nature04614, 2006.
- Yang, X., Pyle, J. A., and Cox, R. A.: Sea salt aerosol production and bromine release: Role of snow on sea ice, *Geophys. Res. Lett.*, 35, L16815, doi:10.1029/2008GL034536, 2008.
- Yung, Y. L., Lee, T., Wang, C.-H., and Shieh, Y.-T.: Dust: A Diagnostic of the Hydrologic Cycle During the Last Glacial Maximum, *Science*, 271, 962–963, doi:10.1126/science.271.5251.962, 1996.